



Understanding the effects of cloud seeding into tropical cyclones using the ICON Model

GEO 511 Master's Thesis

Author: Luis Rivero, 18-102-301

Supervised by: Prof. Dr. Ulrike Lohmann (ulrike.lohmann@env.ethz.ch), Andrina Caratsch (andrina.caratsch@env.ethz.ch)

Faculty representative: Prof. Dr. Jan Seibert

31.07.2025

Contents

1	Introduction	5
1.1	Tropical Cyclones as a Natural Hazard	5
1.2	Structure of TCs and Aerosol Interactions	6
1.3	Cloud Microphysics and the Role of Aerosols in TCs	7
1.4	Artificial TC Modification: Studies	9
1.5	Review of Studies on Artificial TC Modification	10
1.5.1	First Attempts	10
1.5.2	CCN	11
1.5.3	Aerosol Effects in Numerical Simulations	11
1.5.4	Rainfall Modifications and Coastal Flooding	11
1.5.5	Effects on Tracks	12
1.6	Research Gap and Thesis Objectives	12
1.7	Hypothesis and Structure	13
2	Data and Methods	15
2.1	Model Setup	15
2.2	Cloud Microphysics Parameterization	15
2.3	TC Tracking Algorithm	16
2.4	TC Selection	17
2.5	CCN Properties and Injections	18
3	Results	21
3.1	Control Simulation	22
3.2	TC Intensities (SLP) and (v_{\max})	23
3.3	TC Track Deviations	28
3.4	Cloud Droplet Distribution	29
3.5	Cloud Microphysics	30
3.6	Precipitation	34

3.7	Thermodynamics	37
3.8	Wind Fields	41
3.9	Summary of Results	48
4	Discussion and Conclusion	50
4.1	Comparison with the Literature	50
4.2	Limitations	52
4.2.1	Model Noise and Structural Uncertainty	52
4.2.2	Limitations related to Model Performance	53
4.3	On the Idealized Nature of the Seeding Setup	53
4.3.1	Limitations due to Missing Ensemble Simulations	54
4.4	Relevance and Implications	54
4.5	Conclusion and Outlook	55
4.6	Recommendations for Future Research	55
5	Acronyms	62

Abstract

This thesis investigates the microphysical and dynamical responses of tropical cyclones (TCs) to artificial seeding with cloud condensation nuclei (CCN), using high-resolution simulations with the ICON model. Motivated by the hypothesis that aerosol perturbations can modify convective organization, precipitation efficiency, and storm intensity, a set of idealized experiments was designed to inject CCN into different regions of a developing cyclone: the eyewall, the outer periphery, and the entire storm domain. The analysis focuses on thermodynamic structure, updraft strength, hydrometeor distribution, and precipitation patterns throughout the seeding phase and the subsequent evolution.

The results show that seeding effects are sensitive to the injection location. Eyewall seeding leads to enhanced updrafts and temporarily intensified inner-core convection, but reduces rainfall in the outer rainbands. Periphery seeding has the opposite effect: it suppresses rainband updrafts and leads to more disorganized precipitation fields. Total-domain seeding produces a mixed response, partially reinforcing cloud water content without consistent storm intensification. Despite these structural changes, the cyclone tracks remain nearly identical across all simulations, and differences in total accumulated precipitation are subtle. No evidence is found for a systematic weakening or strengthening of the storm due to CCN seeding alone.

This study highlights the complex, non-linear nature of aerosol-cloud interactions in intense convective systems and illustrates both the potential and limitations of geoengineering approaches to tropical cyclone modification.

1 Introduction

1.1 Tropical Cyclones as a Natural Hazard

Tropical cyclones (TCs) pose one of the gravest natural threats to coastal regions, due to extreme winds, storm surges, torrential rainfall, flooding, and occasional tornadoes. On average, around 22 million people are directly affected per year, with annual economic losses reaching approximately 29 billion US-Dollars (Geiger et al., 2018; NOAA, 2025). The impacts of TC's vary significantly by region. In the Global North (e.g., the United States and Japan), TC's represent the natural hazard with the highest economic losses, yet 82% of flood-related damages remain uninsured. In contrast, in the Global South (e.g., the Philippines and Mozambique), TC's pose a greater threat to human lives (SwissRe, 2023). The intertwining of climate change and coastal population growth intensifies these impacts, heightening vulnerability and underscoring the need for improved mitigation strategies (Intergovernmental Panel On Climate Change (IPCC), 2022; Neumann et al., 2015). Due to their devastating impacts on human life, infrastructure, ecosystems, and entire societies in tropical regions, TC's have long been at the center of atmospheric research. Over the past century, our understanding of their structure and dynamics has advanced remarkably. Key milestones include the conceptualization of TC's as heat engines operating akin to a Carnot cycle (Emanuel, 1986), the empirical formulation of wind and pressure profiles (Holland, 1980), the introduction of satellite-based remote sensing and airborne measurements, and the development of sophisticated numerical weather prediction models such as WRF (Skamarock et al., 2019) or ICON (Zängl et al., 2015). Furthermore, global reanalysis datasets have provided consistent, long-term perspectives on storm behavior (Hersbach et al., 2020). Alongside these advancements in observation and modeling, increasing attention has turned toward the role of aerosols—specifically cloud condensation nuclei (CCN)—in shaping the internal dynamics of TCs. To understand how aerosols interact with the TC first a

few basic concepts of how the TC works have to be introduced.

1.2 Structure of TCs and Aerosol Interactions

TCs are intense, organized low-pressure systems with a warm core structure and positive relative vorticity in the lower troposphere (Emanuel, 1986). A mature TC typically exhibits a distinct three-part structure: a calm, nearly cloud-free eye; a surrounding convective eyewall with vigorous updrafts and deep convection; and spiral rainbands that extend outward and modulate the storm’s interaction with its environment (Montgomery & Smith, 2014).

The dominant wind field, known as the *primary circulation*, is governed by a near-gradient wind balance, where the pressure gradient force directed inward is balanced by the outward-directed centrifugal force and the Coriolis force, which acts to the right of the motion in the Northern Hemisphere. In the boundary layer, however, surface friction slows down the wind and alters this balance. The frictional force opposes motion and reduces the tangential wind speed, resulting in an inward-directed radial component in the outer storm (subgradient flow), and outward-directed supergradient flow near the inner core. There where the subgradient and supergradient winds meet is the place of highest wind speed in the whole system. This convergence of airflow forces the air to go upwards inducing the secondary circulation. (Montgomery & Smith, 2014; Smith & Montgomery, 2010).

This radial inflow causes convergence near the eyewall base, leading to intense upward motion. As air rises in the eyewall, it cools and condenses, releasing latent heat. This latent heating increases the buoyancy of the air parcel, reduces local pressure aloft, and reinforces the convective updrafts. The resulting vertical motion sustains the secondary circulation, characterized by upper-level outflow at the tropopause and subsidence in the eye and outer regions (Smith & Montgomery, 2008).

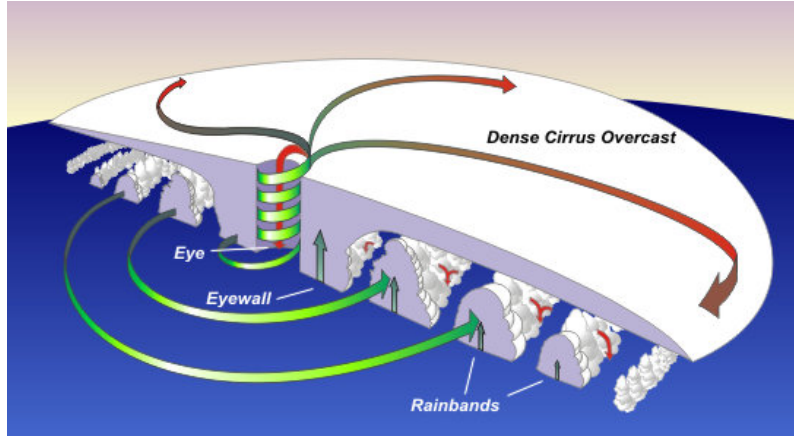


Figure 1: Three-dimensional schematic of a mature TC. The image illustrates the primary (green wind arrows around the TC) and secondary circulation (updrafts in the eyewall and upper-level outflow in the dense cirrus overcast.) Source: NOAA Hurricane Research Division¹

This idealized energy cycle has been likened to a Carnot heat engine, where thermal energy extracted from the warm ocean surface is partially converted into mechanical work—mainly the strong rotational wind field. The rest of the energy is dissipated through surface drag and radiative processes (Emanuel, 1986). In this framework, the air parcel undergoes isothermal expansion while gaining moisture (and θ_e) near the ocean surface, adiabatic ascent in the eyewall (at nearly constant θ_e), radiative cooling and descent in the upper troposphere, and adiabatic warming in the subsiding branches, thereby completing the thermodynamic loop (Montgomery & Smith, 2014). The equivalent potential temperature (θ_e) is a conserved thermodynamic quantity that reflects both temperature and moisture content. It increases during moisture uptake and decreases with radiative heat loss, making it an effective diagnostic for analyzing moist convection and the energetic efficiency of the cyclone system (Emanuel, 1994).

1.3 Cloud Microphysics and the Role of Aerosols in TCs

Beyond the thermodynamic and dynamic framework of TCs, recent research has emphasized the importance of cloud microphysical processes and their sensitivity to

ambient aerosol concentrations—particularly CCN. These submicron particles, originating from natural sources (e.g., sea salt, desert dust) or anthropogenic emissions, act as nucleation sites for cloud droplets when relative humidity exceeds saturation.

An increase in CCN concentration initiates a cascade of microphysical effects that substantially alters convective cloud characteristics:

**Droplet Number $\uparrow \Rightarrow$ Droplet Size $\downarrow \Rightarrow$ Collision–Coalescence Efficiency
 $\downarrow \Rightarrow$ Latent Heat Release $\uparrow \Rightarrow$ Precipitation Efficiency \downarrow**

The key process suppressed in this chain is *collision–coalescence*, which describes the growth of raindrops through the collection of smaller cloud droplets via gravitational settling. In cleaner environments with fewer CCN, droplets grow larger and faster, leading to efficient precipitation. Under high CCN conditions, however, the available water vapor is distributed among many small droplets. These droplets fall at similar terminal velocities and collide less frequently, which inhibits the formation of precipitation-sized drops (Arieli et al., 2025; Rosenfeld et al., 2012). As a result, more cloud water remains in the supercooled state and is transported aloft by updrafts. Upon freezing, this water releases additional latent heat, increasing buoyancy and potentially invigorating vertical motion in convective towers. These feedbacks are at the core of current research into aerosol–convection interactions in TC. This prolongs the cloud lifetime and allows more supercooled liquid water to reach higher altitudes, where freezing releases latent heat that strengthens updrafts. Building on these microphysical insights, recent studies have investigated how aerosol perturbations—particularly changes in CCN concentrations—can modify the intensity and structure of TCs. These investigations indicate that aerosols significantly alter storm dynamics by affecting cloud depth, droplet lifetime, and the vertical distribution of heating. In a TC-specific context, Rosenfeld et al. (2012) showed that this invigoration can lead to deeper and more intense convective towers, particularly in the outer rainbands. The associated redistribution of latent heating may weaken inner-core convection and broaden the storm’s structure. Paradoxically, this can reduce peak

wind speeds while expanding the area of damaging winds. Their simulations and satellite analyses highlight the non-linear nature of aerosol effects and their strong dependence on environmental conditions such as mid-level humidity, CCN concentration, and injection location. Lohmann et al. (2007) show that the response of precipitation to aerosol loading is highly nonlinear. Using cloud-resolving simulations of orographic convection, they find that moderate CCN concentrations can enhance precipitation by invigorating updrafts and increasing ice-phase processes aloft. However, very high CCN levels suppress rain formation due to inhibited collision-coalescence and enhanced condensate loading, which ultimately weakens the updrafts. This threshold behavior highlights the need to interpret aerosol effects in a context-dependent and non-monotonic manner.

1.4 Artificial TC Modification: Studies

Inspired by the insights into microphysical mechanisms inside TCs, the scientific community has long been interested in artificially modifying TCs to reduce their destructive potential. The motivations for such interventions are diverse such as:

- **Mitigation of Human and Economic Losses:** As discussed previously the, TCs cause extensive damage to infrastructure and lead to thousands of deaths annually. Modifying storm intensity or structure could protect densely populated coastal areas and reduce insurance losses, especially in regions lacking resilient infrastructure.
- **Complementary Disaster Risk Management:** Even with accurate forecasting, TCs remain difficult to manage. Targeted storm manipulation might provide additional time for evacuation or lessen the impact where traditional mitigation strategies (e.g., seawalls or retreat) are infeasible.
- **Scientific Advancement:** Artificial interventions enable controlled experimentation to improve our understanding of aerosol-cloud interactions, con-

vective processes, and TC dynamics. This contributes to refining numerical weather prediction models.

- **Geoengineering and Climate Adaptation:** As climate change is expected to intensify TCs through rising sea surface temperatures, storm modification is increasingly discussed in the context of long-term geoengineering. CCN injections may serve as a prototype for broader atmospheric intervention technologies.

1.5 Review of Studies on Artificial TC Modification

Over the past decades, numerous scientific studies have explored the potential to artificially modify TCs. The approaches range from historical field experiments to idealized numerical simulations and satellite-based observational analyses. The findings suggest a complex and often contradictory picture: while certain configurations appear to weaken TCs, others may unintentionally enhance their intensity. Below is an overview of major studies, organized by methodological approach and main findings.

1.5.1 First Attempts

The STORMFURY project (Willoughby et al., 1985) was a pioneering field campaign aimed at weakening TC by cloud seeding with silver iodide as injection agent. The strategy intended to induce ice formation in supercooled water outside the eyewall to shift convection radially outward. Smith (1981) theorized that expanding the eye would reduce wind speeds due to the conservation of angular momentum and a weaker horizontal pressure gradient.

Although temporary reductions in wind speed were reported, the project ultimately failed due to an insufficient amount of supercooled water in most TCs. Furthermore, the intended effects closely resembled the naturally occurring *eyewall replacement cycle* (ERC), wherein a secondary eyewall forms and gradually replaces

the primary one (Kossin & Sitkowski, 2012; Willoughby et al., 1981; Zhou & Wang, 2011).

1.5.2 CCN

The role of aerosols in cloud microphysics has been well documented (Lohmann & Feichter, 2005). High CCN concentrations produce numerous small droplets that suppress warm rain formation via collision-coalescence, prolong cloud lifetime, and increase cloud albedo (Twomey effect). Updrafts can carry these small droplets to supercooled levels, where freezing releases latent heat and invigorates convection (Carrio & Cotton, 2011; Rosenfeld et al., 2012).

1.5.3 Aerosol Effects in Numerical Simulations

Several modeling studies (e.g., using WRF and RAMS) investigated aerosol effects on TC structure and intensity. Rosenfeld et al. (2007) simulated Hurricane Katrina and found that aerosol-induced convection in peripheral rainbands suppressed mass flux into the eyewall, weakening central convection. Khain et al. (2008) and Zhang et al. (2007) and Hazra et al. (2013) reported similar results: aerosol-induced peripheral convection disrupted warm moist inflow to the core, reducing intensity.

Conversely, other studies found that aerosol intrusion into the eyewall can strengthen TCs. Liang et al. (2021) and Herbener et al. (2014) demonstrated that aerosols can suppress warm rain formation in the core, allowing supercooled water to be lofted and release latent heat upon freezing, thereby intensifying convection and enhancing vortex stretching.

1.5.4 Rainfall Modifications and Coastal Flooding

Satellite studies using MODIS and TRMM/GPM Zhao et al. (2018) showed that aerosol intrusion can enhance outer rainband convection, potentially increasing total rainfall area and amplifying coastal flood risks. Jiang et al. (2016) found that in

highly polluted cases, precipitation was suppressed due to inhibited autoconversion processes, reducing rainfall efficiency.

Conversely, Ghosh et al. (2016) proposed seeding the TC eyewall with giant CCN prior to landfall. Larger droplets promoted warm rain processes such as collision-coalescence, enhancing rainfall before landfall and potentially reducing the flood threat during impact.

1.5.5 Effects on Tracks

The potential for aerosol-induced TC track changes remains controversial. Modeling studies (Jiang et al., 2016; Lin et al., 2011) found no consistent evidence of trajectory alteration. A notable historical case occurred in 1947, when a dry ice-seeded storm made an unexpected landfall in the U.S. (Willoughby et al., 1985).

This incident highlights the ethical and societal implications of artificial storm modification and the need for cautious interpretation of cause and effect.

Summary

The reviewed studies collectively suggest that aerosol-TC interactions are highly context-dependent. Effects vary with aerosol type, injection location, storm stage, and environmental conditions. While weakening is possible via peripheral convection enhancement, the potential for unintended intensification—especially near the eyewall—remains a critical concern. Further ensemble modeling and multi-model intercomparison studies are essential to constrain the uncertainty in aerosol-TC interaction pathways.

1.6 Research Gap and Thesis Objectives

Despite growing interest in aerosol-based TC modification, substantial uncertainties remain regarding how CCN injections influence storm structure, thermodynamics, and intensity. Existing studies are often limited to single-case analyses, do not

systematically compare seeding regions, or employ models with insufficient spatial or microphysical resolution. Moreover, many experiments conflate dynamic and thermodynamic feedbacks, preventing a clear attribution of observed effects.

To address these limitations, this study conducts a high-resolution sensitivity analysis using the ICOSahedral Nonhydrostatic (ICON) model. It systematically investigates how the spatial placement of artificial CCN injections—in the eyewall, the periphery, or the full storm domain—modulates the structural evolution, intensity, and energy distribution of a developing TC. By isolating the seeding impact under idealized yet physically realistic conditions, the study aims to advance our understanding of aerosol–convection interactions and to critically assess the feasibility of targeted storm modulation strategies.

The overarching objective is to quantify how localized CCN injections affect the dynamic, thermodynamic, and microphysical structure of a TC. This is achieved through a controlled set of simulations that analyze changes in variables such as cloud droplet number concentration (q_{nc}), cloud water and ice content (q_c , q_i), vertical velocity (w), equivalent potential temperature (θ_e), precipitation rate ($prec$), and wind components (v_r , v_t). The central research question is formulated as follows:

How does the spatial location of artificial CCN injection influence the structural evolution and intensity of a TC?

Through this targeted sensitivity experiment, the study contributes to the physical basis for evaluating the prospects and limitations of aerosol-based TC modification, while also clarifying how different seeding strategies interact with internal storm dynamics.

1.7 Hypothesis and Structure

Hypothesis *Cloud seeding in the eyewall is expected to intensify vertical motion through enhanced latent heat release, whereas peripheral seeding is hypothesized to suppress core convection by modifying thermodynamic gradients and inflow characteristics.*

The structure of this thesis is as follows: Chapter 2 describes the modeling framework, including microphysical parameterizations, TC tracking algorithms, case selection, and the design of the CCN seeding experiments. Chapter 3 presents the outcomes of both the control simulation and the sensitivity experiments, focusing on storm responses in terms of pressure, wind structure, microphysical properties, thermodynamic fields, and precipitation. Chapter 4 interprets these findings in the context of existing literature, discusses associated uncertainties, evaluates their generalizability, and concludes with recommendations for future research and geo-engineering considerations.

2 Data and Methods

2.1 Model Setup

The experiments were conducted using ICON (Zängl et al., 2015)(version 2.6.4) (Icosahedral Nonhydrostatic), a numerical weather prediction model based on non-hydrostatic equations and an icosahedral grid. The model domain is centered over the North Atlantic Basin, spanning latitudes from 0° to 70°N and longitudes from 15°W to 120°W , located in the main TC developing region of the North Atlantic Ocean. Vertically, ICON is discretized by 50 levels, with the resolution decreasing with altitude. 6-hourly lateral boundary conditions were derived from ERA5 reanalysis data provided by the ECMWF (Hersbach et al., 2020). Sea surface temperature and sea ice concentration were prescribed using daily interpolated values of a monthly averaged dataset. The horizontal grid spacing is 0.125° (approx. 13km) and the model time step is 50 seconds. Output data are available at six-hour intervals (0000, 0600, 1200, and 1800 UTC), with the variables: zonal, meridional, and vertical wind components, pressure, temperature, specific humidity, grid-scale precipitation rate (prec), and cloud cover. The simulation period spans from 1 August to 31 August 2005 - a month selected for its historically high TC activity, including notable storms such as Hurricanes Wilma and Katrina (Beven et al., 2008). This setting increases the likelihood of generating intense and well-organized storms. The convection parameterization was disabled, so that cloud formation is sensitive to injected CCN-Particles.

2.2 Cloud Microphysics Parameterization

Cloud microphysical processes are simulated using the two-moment scheme developed by (Seifert & Beheng, 2006), which prognoses both mass mixing ratios and number concentrations for five hydrometeor categories: cloud droplets, rain, ice crystals, snow, and graupel. The scheme explicitly links the cloud droplet num-

ber concentration to the ambient CCN concentration, thereby allowing a dynamic response to aerosol perturbations. Droplet activation is parameterized following Köhler theory, using a simplified analytical approximation that relates the number of activated droplets to supersaturation and CCN properties (e.g., size distribution, hygroscopicity) (**lohmann2005global**). This formulation enables a physically consistent representation of aerosol–cloud interactions in large-scale models without resorting to computationally expensive bin-resolved microphysics. In contrast to spectral bin models that explicitly resolve the size distribution of aerosol and cloud particles (**segal2006droplet**), this approach offers a computationally efficient yet physically grounded means of representing the first aerosol indirect effect.

2.3 TC Tracking Algorithm

To identify storms in the model output, the TC tracking algorithm described by (Enz et al., 2023) is applied to every individual experiment. The algorithm is specifically designed to detect and track TCs in the ICON model output using a combination of physical criteria and a flexible threshold-based approach. This algorithm varies key parameters in parallel, allowing it to detect TCs across a wide range of intensities and developmental stages, including weak or transitioning systems. The tracking procedure is based on three fundamental criteria:

- a local minimum in mean sea level pressure (MSLP) within a radial distance r_m ,
- a positive maximum in lower-tropospheric relative vorticity (evaluated at approximately 750 hPa),
- the presence of a warm core, indicated by a positive temperature anomaly at 300 hPa relative to the surrounding environment.

For each of these criteria, multiple threshold values are defined, ranging from conservative to permissive, and evaluated in parallel. This allows for the detection of

both strong and weak cyclonic systems while minimizing the risk of false positives.

The detection process is conducted individually at each time step. Grid points that meet all criteria are marked as potential TC centers. In a second step, these centers are linked in consecutive time steps to continuous tracks, assuming a maximum translation speed of 25 ms^{-1} . Tracks must persist for at least 12 hours (four time steps) to be retained, which helps filter out transient or spurious features.

Each detected system is evaluated by how many combinations of threshold parameters identify it. A higher detection percentage suggests greater confidence. Tracks are only accepted if they meet the minimum detection thresholds:

- 10 % for tropical depressions
- 20 % for tropical storms
- 50 % for TCs

In general, this algorithm provides a reliable basis for identifying and tracking simulated TCs.

2.4 TC Selection

The TC tracker algorithm detected a total of 128 storms in the control simulation. From these one TC was selected for the seeding experiments. Of the 128 storms, 28 were classified as tropical storms, five as TC, and three reached major TC intensity (Category ≥ 3) (see Figure 2). Figure 1 shows the tracks of all TC generated in the control simulation. Among them, three reached major TC intensity: TC 3 (Category 4), TC 31 (Category 3), and TC 77 (Category 3). TC 3 was the only system to make landfall; the other two remained entirely over the open ocean. The limited land interaction and clear intensification pattern to a major TC category make this cyclone an ideal candidate for CCN perturbation experiments. Moreover, the realistic scenario of a major natural hazard threatening a densely populated,

multi-million metropolitan area (Miami metropolitan area) adds further relevance to the case study.

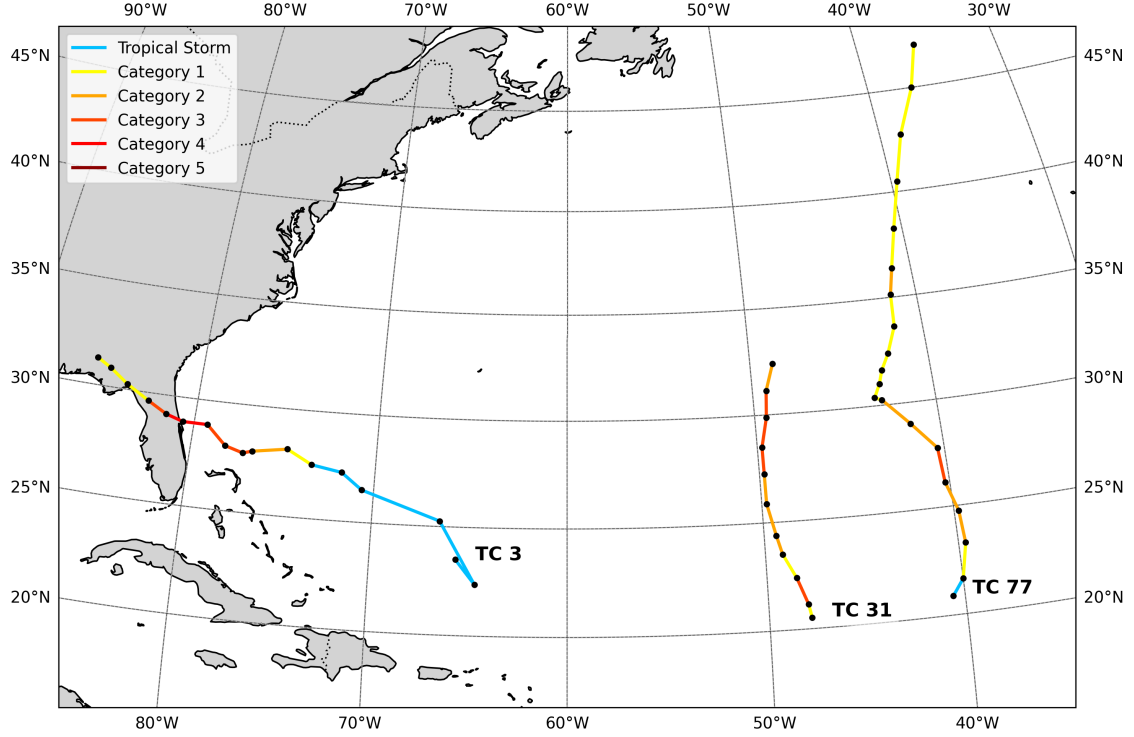


Figure 2: Tracks of TC generated in the control simulation. A total of three storms reached major TC intensity (Category ≥ 3) and were considered as candidates for the seeding experiments: TC 3 (Category 4), TC 31 (Category 3), and TC 77 (Category 3). TC 3 is the only storm making landfall while the other two remain completely in the open ocean.

2.5 CCN Properties and Injections

The background concentration of CCN is 100 cm^{-3} for the fulldomain, representative for clean maritime conditions (Segal & Khain, 2006). The aerosol is characterized by a median dry radius $r_m = 0.03 \mu\text{m}$, a geometric standard deviation of $\sigma_s = 0.4$ and a soluble fraction of $\eta = 0.9$, where η denotes the mass fraction of soluble material (Segal & Khain, 2006). This aerosol properties were used consistently across all experiments. The number, vertical height, location, and duration of the injections vary between the individual experiments and are further described in the following chapter in detail.

All perturbation experiments were conducted using three distinct seeding regions (see Fig. 3). The seeding domains were defined based on radial distance from the storm center: (1) *Total Seeding* (0–500 km), (2) *Eyewall Seeding* (0–80 km), and (3) *Periphery Seeding* (120–500 km).

To ensure a clear separation between the eyewall and periphery regions, a 40 km buffer zone between 80 km and 120 km was intentionally left unseeded. This gap minimizes overlap and allows for a more unambiguous attribution of any resulting storm modifications to either the inner-core or outer-region aerosol forcing.

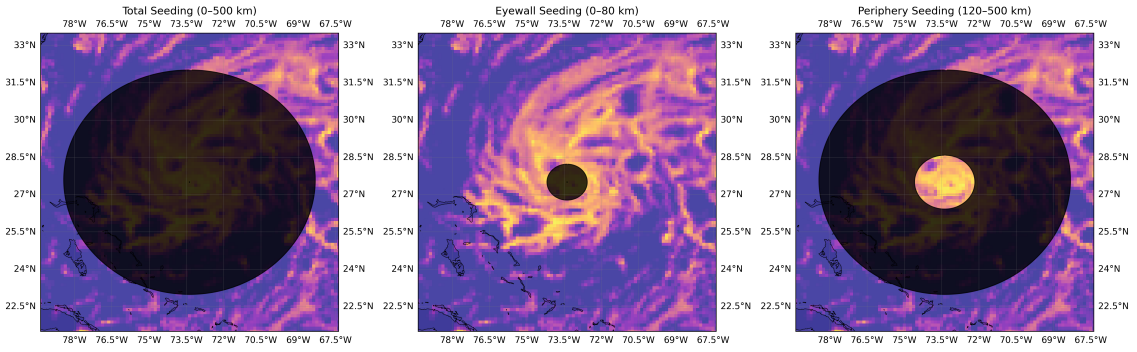


Figure 3: Visualization of seeding zones for the sensitivity analysis. The simulated cloud cover (%) at 500 m above sea level is shown in the background, overlaid with the three seeding domains: Total Seeding (0–500 km), Eyewall Seeding (0–80 km), and Periphery Seeding (120–500 km). Black areas indicate the respective aerosol injection regions. The colors in the background show the vortex of the selected TC. Purple colors are low velocities and yellow colors are high velocities.

Preliminary tests were conducted to identify sensitivities, determine the seeding height and duration for the experiments. Based on these experiments and the findings of Chan (2023), which suggest that CCN must be activated below cloud base to effectively influence cloud microphysics, the seeding was performed at a height of 294 meters above sea level. The injection duration was set to six hours, from August 18 at 06:00 UTC to 12:00 UTC. This timing corresponds to a phase in which the cyclone had already reached TC intensity and featured a well-developed inner-core structure, including an identifiable eyewall, but had not yet reached its maximum intensity (Category 4), which as of the goal of this thesis is to be mitigated.

For each of the three seeding configurations—total (0–500 km), eyewall (0–80 km),

and periphery (120–500 km)—a set of four perturbation experiments was performed with increasing CCN injection rates of $20\,000\text{ cm}^{-3}\text{ s}^{-1}$, $200\,000\text{ cm}^{-3}\text{ s}^{-1}$, and $2\,000\,000\text{ cm}^{-3}\text{ s}^{-1}$, respectively. This resulted in a total of twelve simulations. All runs were initialized with identical boundary conditions derived from ERA5 reanalysis data and differed only in their aerosol seeding configurations.

Table 1: Naming scheme for the twelve seeding experiments. Rows indicate the seeding region; columns indicate the CCN injection rate. The shorthand labels (e.g., 2e4e) combine the CCN concentration and the seeding domain: e = Eyewall, p = Periphery, t = Total.

Seeding Region	2e4 $\text{cm}^{-3}\text{ s}^{-1}$	2e5 $\text{cm}^{-3}\text{ s}^{-1}$	2e6 $\text{cm}^{-3}\text{ s}^{-1}$
Eyewall (e)	2e4e	2e5e	2e6e
Periphery (p)	2e4p	2e5p	2e6p
Total (t)	2e4t	2e5t	2e6t

3 Results

This chapter begins with a brief overview of the control simulation. Starting from Section 4.1, the seeding experiments are described, analyzed, and compared to the control run. The analysis is structured according to the following variables and aspects of the TC's:

- Pressure and maximum wind speed (Section 3.2)
- Cyclone tracks (Section 3.3)
- Cloud droplet distribution (Section 3.4)
- Cloud microphysics (q_c and q_i)(Section 3.5)
- Precipitation(Section 3.6)
- Thermodynamics (θ and θ_e) (Section 3.7)
- Wind field components (radial, tangential, and vertical) (Section 3.8)

Up to Section 3.3, the results of all experiments are discussed to provide a comparative overview. Section 3.4 focuses on the distribution patterns of cloud droplet number concentrations (CDNC) in the low-intensity seeding cases (2e4t, 2e4e, and 2e4p), highlighting the spatial response under minimal aerosol injections. From Section 3.5 onward, the analysis shifts to the 2e6 injection experiments, which exhibit the most pronounced differences—particularly in the periphery case (2e6p). The results chapter will be summarized in the subsection 3.9

Together, these analyses aim to determine whether seeding TC with CCN leads to discernible changes in their thermodynamic and dynamical evolution as simulated by the ICON model.

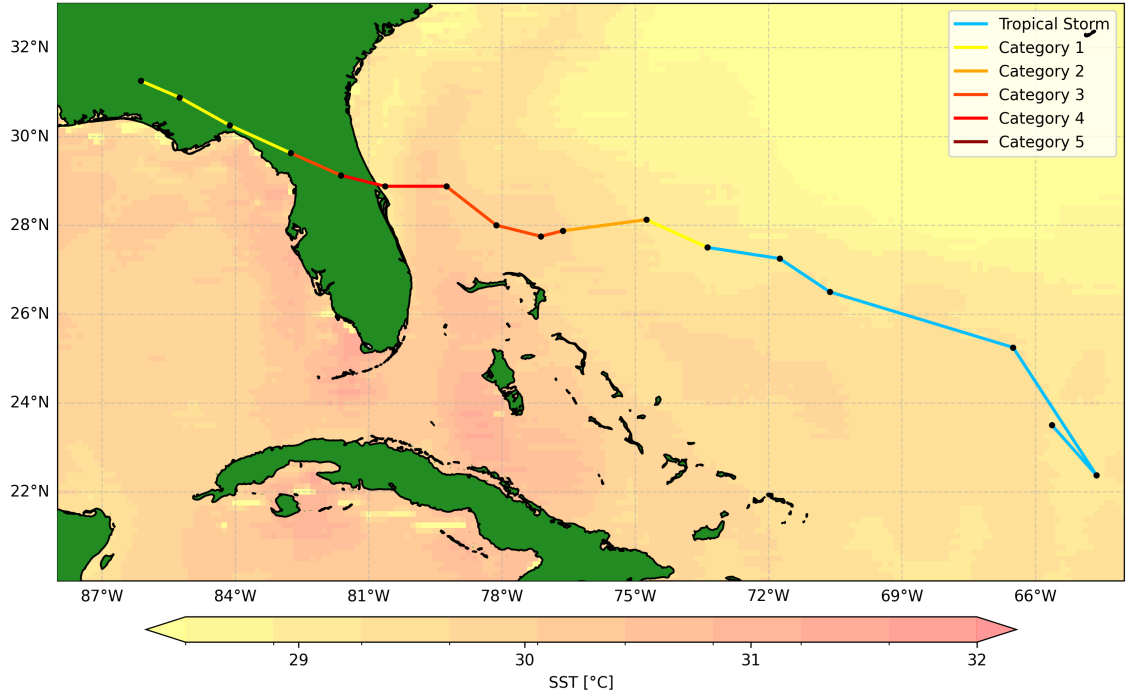


Figure 4: Track of the selected TC with sea surface temperatures (SST) in the Caribbean Sea and North Atlantic. The cyclone’s intensity is color-coded according to the Saffir-Simpson scale, ranging from tropical storm (blue) to Category 5 (dark red). SST is shown in °C.

3.1 Control Simulation

The selected TC (No. 3), (see Fig. 4) formed over the central North Atlantic near 22°N, 66°W. The TC followed a long uninterrupted oceanic path with sea surface temperatures (SST) consistently above 28.5 °C, two degrees above the necessary 26.5° C for tropical storm formation, which favors continuous intensification. It moved steadily west-northwestward, gradually intensifying. The storm first reached TC strength northeast of the Bahamas and later intensified to Category 3 and Category 4 as it moved north of the Florida Strait. Landfall occurred at Cape Canaveral on Florida’s east coast. The storm then weakened while progressing northwestward across the Florida Peninsula, dissipating over land. Throughout its development, the storm remained in a purely maritime aerosol environment with a prescribed CCN concentration of 100 cm^{-3} . It reached its peak intensity on 19 August at 18:00 UTC, with maximum wind speeds of 63 m s^{-1} (Category 4) and a

minimum central pressure of 946.93 hPa, just before landfall.

3.2 TC Intensities (SLP) and (v_{\max})

In terms of pressure, all perturbed TCs exhibit an increase in minimum sea level pressure (SLP), compared to the control simulation. The smallest increase is 3 hPa in experiment 2e4e, while the largest is 12 hPa in 2e5t and 2e5e. The strongest pressure responses occur in the 2e5 perturbations for the total and eyewall seeding experiments, while in the periphery cases, the most significant changes are seen in the 2e6 perturbations. With regard to maximum wind speed, the response is more variable and does not show a consistent trend of intensity reduction across all cases. All experiments maintain the same TC intensity as the control, except 2e6t, which intensifies to Category 5. In contrast, configurations such as 2e5e, 2e4p, and 2e5t show a pronounced decrease in wind speed, approaching Category 3 intensity.

To provide an overview of the sensitivity of the experiments to spatially distinct CCN injections, the temporal evolution of maximum wind speed (v_{\max}) and sea level pressure (SLP) is shown in Figures 6–5.

Periphery Seeding: Aerosol injections into the rainbands (Figure 5) result in a noticeable divergence between the control and perturbed simulations shortly after the seeding interval. In all perturbation cases, v_{\max} decreases, in contrast to the continued intensification observed in the control run. Temporarily, all three experiments drop by one category on the Saffir–Simpson scale (from Category 3 to 2) between 18 August 18:00 UTC and 19 August 18:00 UTC. After this weakening phase, experiments 2e4p, 2e5p, and 2e6p return to control-level values, but do not overshoot as observed in the total seeding scenario. The minimum SLP remains close to, or slightly higher than, the control values, yet with a clearly visible offset.

Total Seeding: The response in the full-domain seeding experiments (Figure 6) is pronounced, both in terms of magnitude and in comparison to the other configurations. Experiments 2e4t and 2e6t initially show a reduction in intensity—particularly

in SLP—within 12 hours after seeding. However, both subsequently intensify more strongly than the control simulation roughly six hours later. Among all experiments, 2e6t produces the highest maximum wind speed (70.5 m s^{-1}), reaching Category 5 intensity. The v_{max} peak occurs earlier and is more pronounced than in the control, while the corresponding minimum SLP is higher. Experiment 2e5t deviates from this pattern and continues to intensify until the TC tracking algorithm fails, leading to data exclusion.

Eyewall Seeding: In the eyewall seeding experiments, the responses are the weakest among all seeding strategies. All perturbations—regardless of injection strength—end to recover toward control-like behavior. The SLP and v_{max} trajectories in all runs closely follow those of the control, with the exception of a slight deviation in the strongest injection case (2e6e), which shows an initial weakening followed by a modest intensification. Although all simulations experience a rise in minimum SLP, experiments 2e4e and 2e6e remain closest to the control. Both the minimum SLP and v_{max} remain slightly above those of the control throughout the post-seeding period.

Overall, the signal from CCN injections is strongest in the periphery seeding experiments, as evidenced by larger deviations and a noticeable flattening in both v_{max} and SLP toward the center of the graph. In contrast, the eyewall case shows little to no response, while the total seeding experiments exhibit a strong initial reaction followed by a pronounced overshoot beyond control levels.

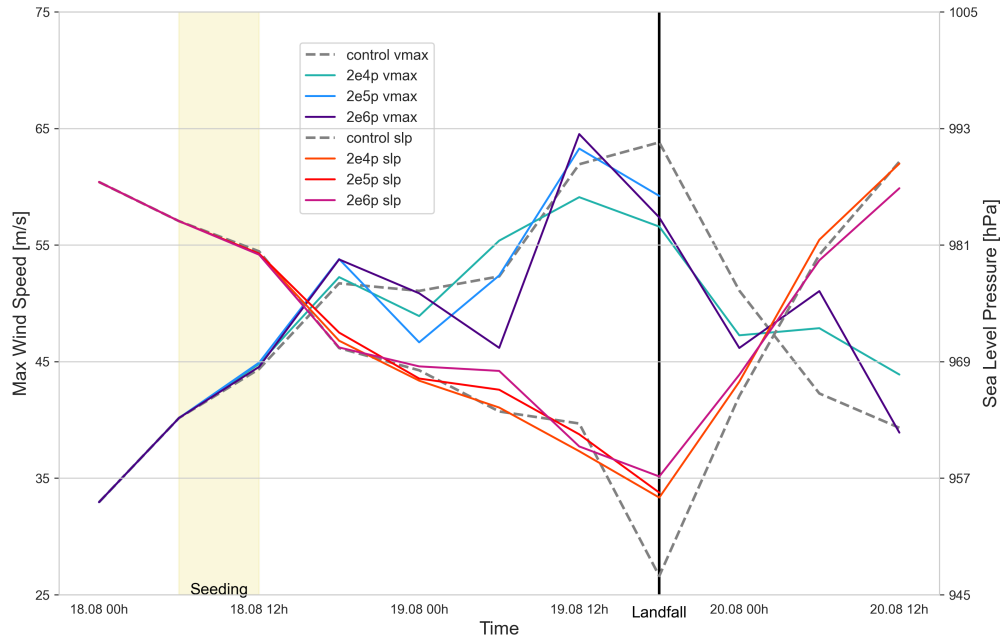


Figure 5: Temporal evolution of sea-level pressure (SLP, red shades) and maximum wind speed (vmax, blue shades) for all experiments with aerosol seeding applied from 120 to 500 km (periphery case) radial distance. Dashed grey lines represent the control simulation. The light yellow area marks the seeding period. Different color shades indicate the respective injection intensities. Due to misalignments in the TC tracking algorithm for experiment 2e5p after August 20, 2005, 00:00 UTC, the corresponding data no longer reflect the actual storm center and were therefore excluded from this figure.

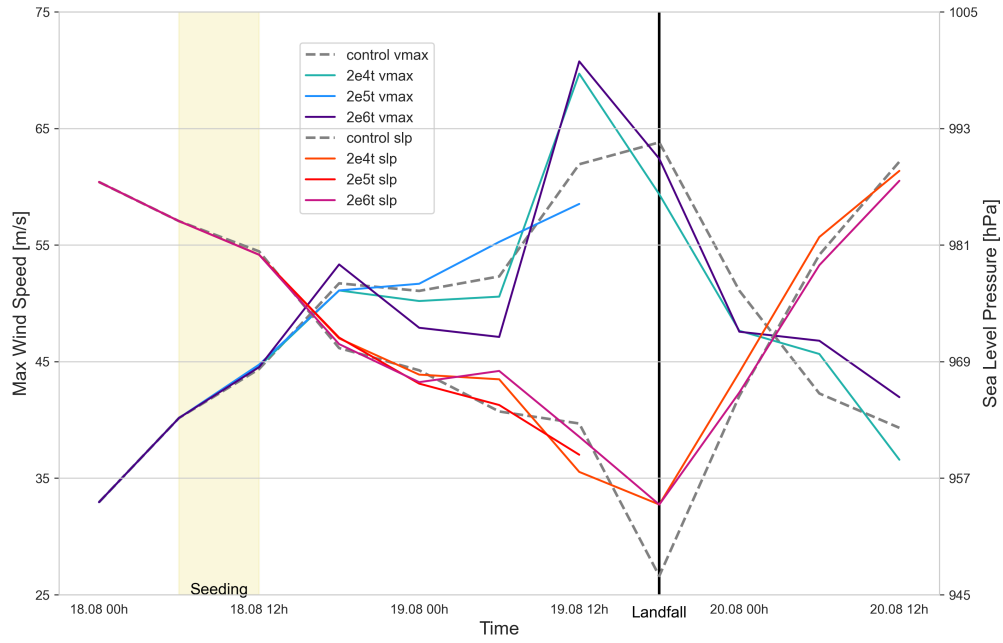


Figure 6: Temporal evolution of sea-level pressure (SLP, red shades) and maximum wind speed (vmax, blue shades) for all experiments with aerosol seeding applied from 0 to 500 km (total case) radial distance. Dashed grey lines represent the control simulation. The light yellow area marks the seeding period. Different color shades indicate the respective injection intensities. Due to misalignments in the TC tracking algorithm for experiment 2e5t after August 19, 2005, 18:00 UTC, the corresponding data no longer reflect the actual storm center and were therefore excluded from this figure.

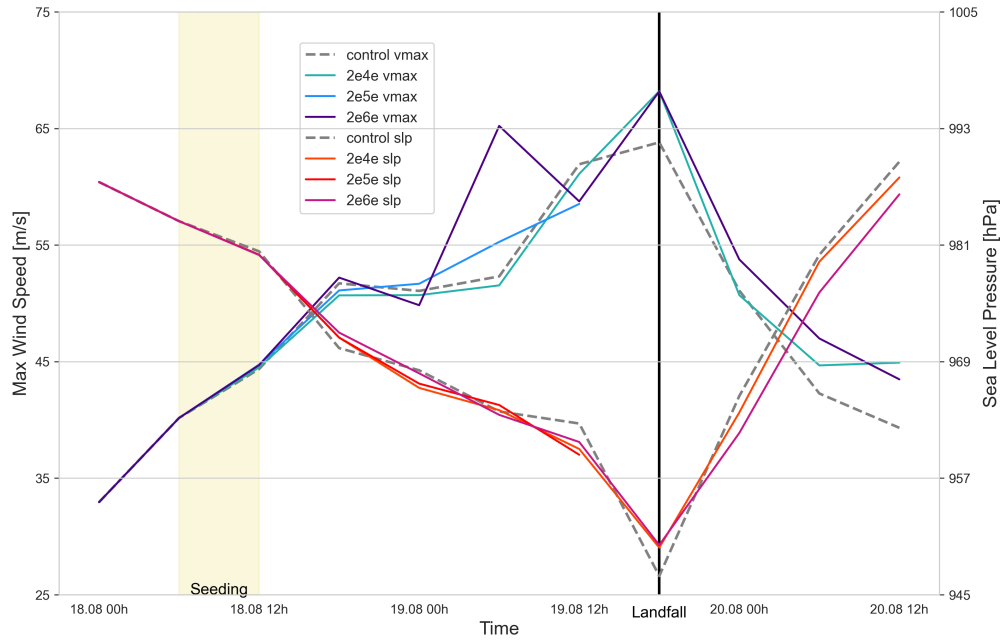


Figure 7: Temporal evolution of sea-level pressure (SLP, red shades) and maximum wind speed (vmax, blue shades) for all experiments with aerosol seeding applied from 0 to 80 km (eyewall case) radial distance. Dashed grey lines represent the control simulation. The light yellow area marks the seeding period. Different color shades indicate the respective injection intensities. Due to misalignments in the TC tracking algorithm for experiment 2e5e after August 19, 2005, 18:00 UTC, the corresponding data no longer reflect the actual storm center and were therefore excluded from this figure.

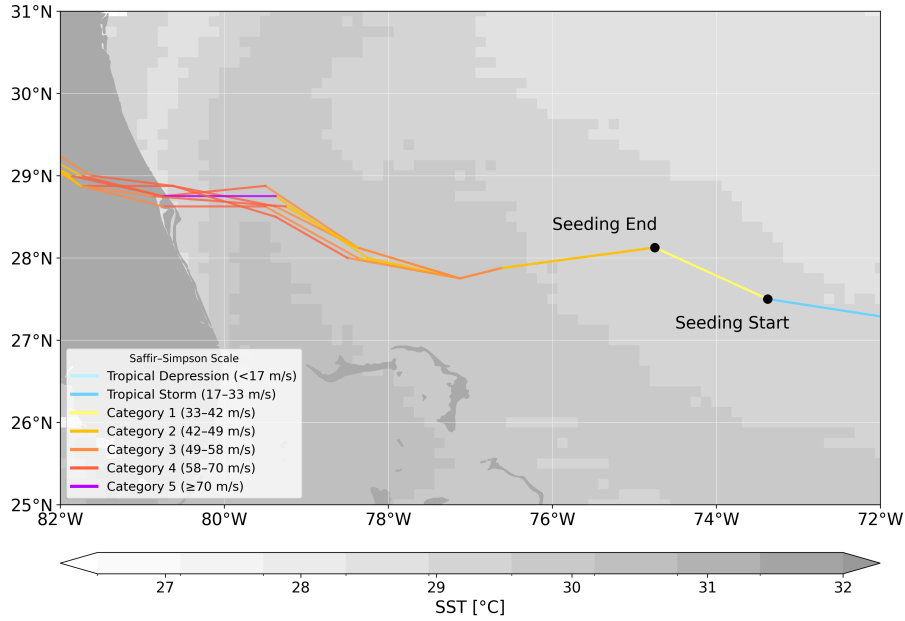


Figure 8: Tracks of all simulated TCs during the seeding and intensification phase shortly before landfall, overlaid on sea surface temperature (SST). The trajectories are color-coded according to the Saffir–Simpson scale based on maximum wind speed. Black dots indicate the start and end points of the CCN injection period. Background shading represents average SST in °C over the period between August 17th 2005 and August 20th 2005. Again, the tracks of 2e5t, 2e5e and 2e5p have been excluded due to mislocation by the track algorithm.

3.3 TC Track Deviations

Figure 8 shows the simulated cyclone tracks after the seeding phase. No significant trajectory deviations are found among the seeding configurations. All storms follow a west-northwestward path and make landfall within a narrow 100 km coastal corridor.

Sea surface temperatures (SST) along the tracks remain nearly identical, as expected from the prescribed, uncoupled SST fields. This supports the conclusion that storm motion is primarily governed by internal dynamics. Under the given model setup, neither SST nor CCN injections significantly affect the large-scale steering flow or storm trajectory.

3.4 Cloud Droplet Distribution

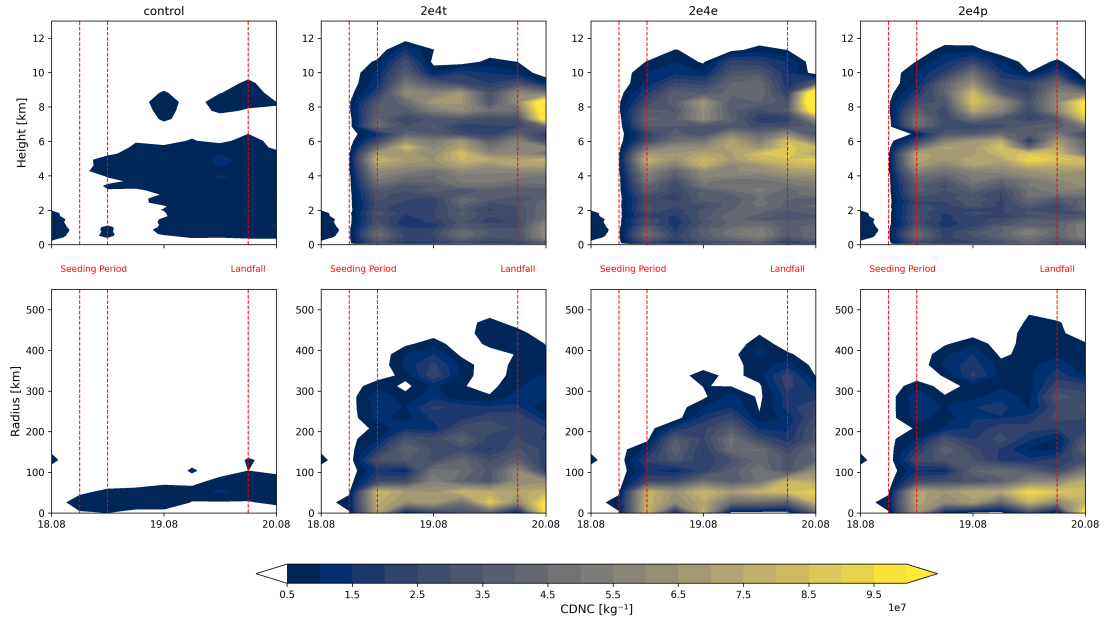


Figure 9: Hovmöller diagrams of cloud droplet number concentration (CDNC) in kg^{-1} for the control experiment and three different seeding experiments (2e4t, 2e4e, 2e4p). The upper row shows the temporal evolution at a fixed radial distance ($r = 60 \text{ km}$) as a function of height, while the lower row displays the evolution at a fixed height ($z = 5 \text{ km}$) as a function of radius. Red dashed lines indicate the beginning and end of the seeding period as well as the time of landfall. The color scale is consistent across all panels and ranges from 5×10^6 to $1 \times 10^8 \text{ kg}^{-1}$.

To assess whether and how the signal of the seeded particles were distributed in the TC and where CCN were activated, Figure 9 presents Hovmöller diagrams of cloud droplet number concentration (CDNC) for four selected experiments: control group, 2e4t (total injection), 2e4e (eye injection), and 2e4p (peripheral injection).

The upper row of the figure shows the vertical distribution of CDNC over time at a fixed radial distance of 56 km from the storm center (approximately within the eyewall). The lower row displays the radial distribution at a constant height of 5 km. All plots cover the period from 18 to 20 August 2005, with red dashed lines indicating the start and end of the seeding phase, as well as the time of landfall.

As expected, the control case shows consistently low CDNC values due to the absence of artificial CCN injections. In all seeded scenarios, enhanced concentra-

tions levels appear in the upper troposphere shortly seeding below cloud base. This indicates that the injected CCN are effectively transported upward and activated within the cloud column during the seeding period.

The vertical profiles of the 2e4t and 2e4e experiments display layered structures with CDNC maxima typically between 5 and 8 km. These layers persist beyond the active seeding window, suggesting sustained activation and vertical redistribution through storm dynamics. This mid-tropospheric peak of CDNC enhancement aligns with expectations: strong updrafts in the eyewall favor supersaturation, droplet formation and vertical transport of cloud droplets into the upper troposphere.

In the 2e4p run, vertical enhancement occurs similarly but with a slight delay in the eyewall region due to the absence of direct seeding there. However, the strong secondary circulation of the TC likely enables rapid inward advection of CCN from the periphery toward the storm center, providing CCN for CDNC formation also in the eyewall.

In the radial dimension, 2e4t and 2e4p show comparable distributions, with high CDNC extending across the inner 150–200 km. In contrast, 2e4e lags behind in the outer regions, again due to the lack of peripheral injection.

Overall, the figure shows that seeding leads to more cloud droplet activation. However the seeding pattern does not cause a large difference in CDNC distribution.

3.5 Cloud Microphysics

Specific Cloud Water Content (Δq_c) (Figure 10): At 06:00 UTC, all three seeding configurations exhibit increased cloud liquid water content (green shading), particularly within the eyewall region. Additional enhancements are also visible in the outer rainbands. Among the experiments, the total seeding case shows the most pronounced increase, while the eyewall case displays the weakest response. The periphery case produces the most spatially extensive anomaly, whereas the eyewall experiment yields a more localized enhancement near the storm core. This

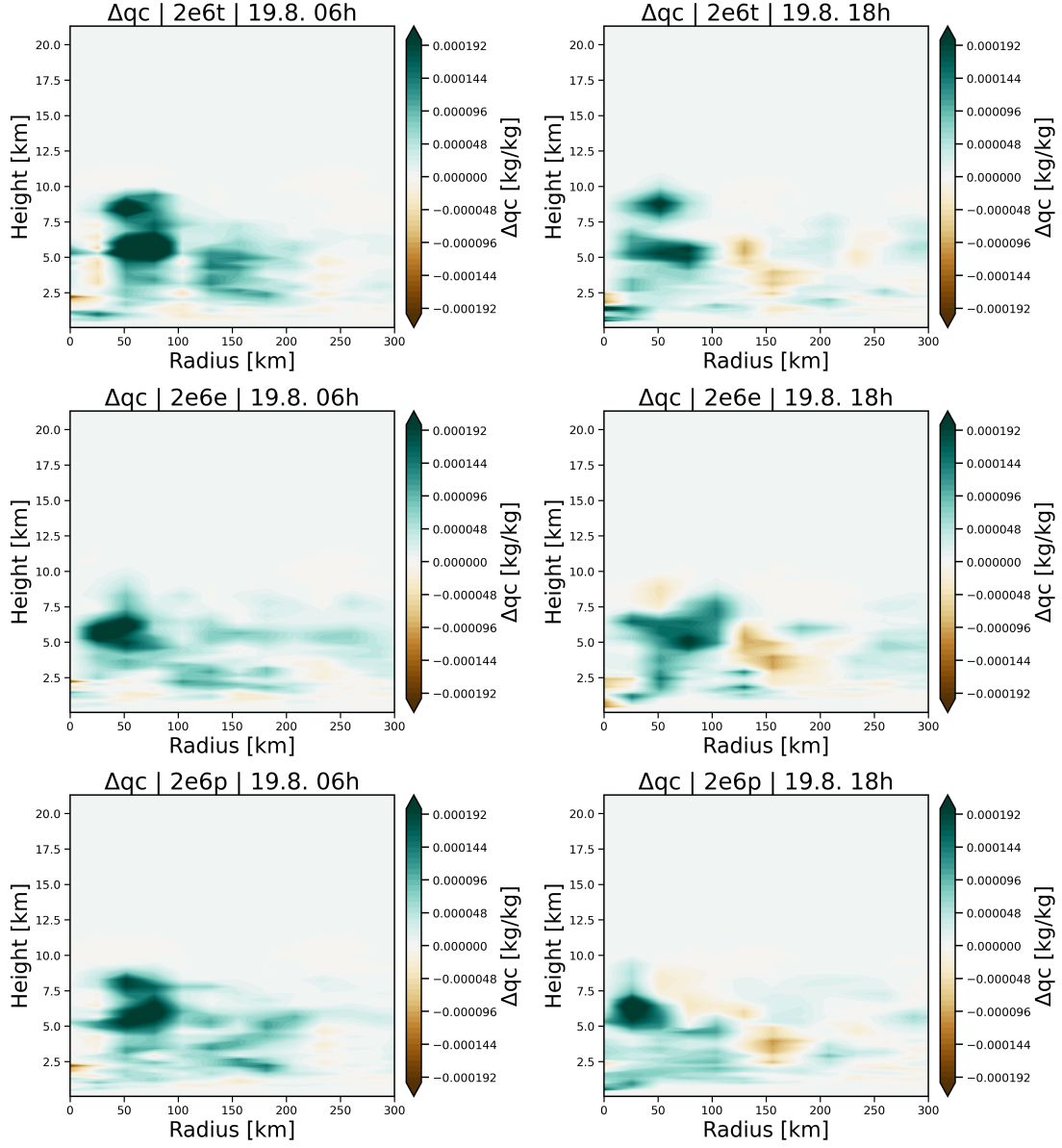


Figure 10: Difference in cloud liquid water content (q_c) between seeded and control simulations for the strongest seeding experiments ($2 \times 10^6 \text{ cm}^{-3} \text{ s}^{-1}$) at 06:00 UTC (left column) and 18:00 UTC (right column) on 19 August 2005. Rows correspond to the three seeding regions: total (top), eyewall (middle), and periphery (bottom). Positive values (green) indicate enhanced liquid water content relative to the control simulation, while negative values (brown) indicate reduced liquid water content.

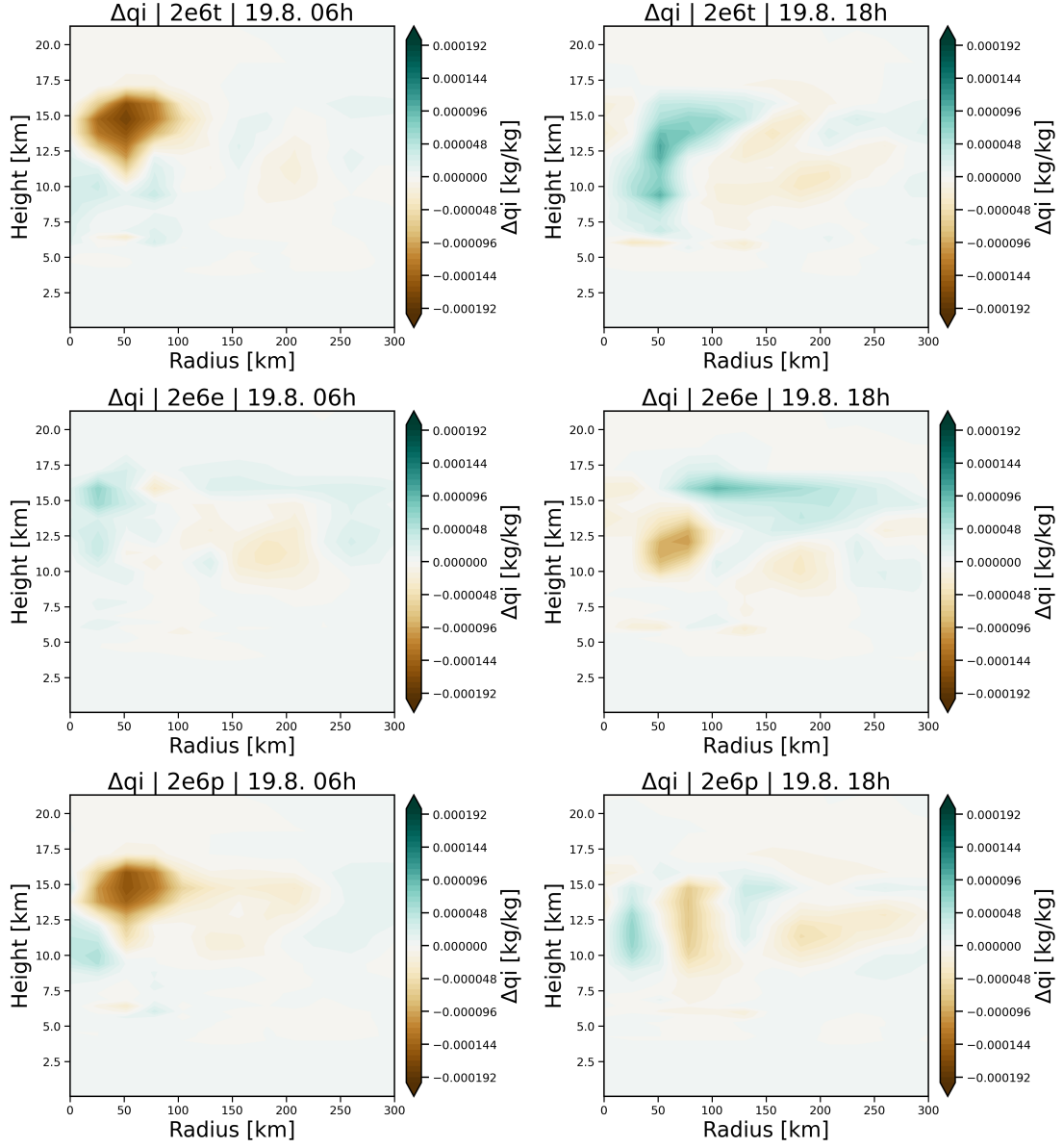


Figure 11: Difference in cloud ice content (q_i) between seeded and control simulations for the strongest seeding experiments ($2 \times 10^6 \text{ cm}^{-3} \text{ s}^{-1}$) at 06:00 UTC (left column) and 18:00 UTC (right column) on 19 August 2005. Rows correspond to the three seeding regions: total (top), eyewall (middle), and periphery (bottom). Positive values (green) indicate enhanced cloud ice formation due to increased glaciation or lofting, while negative values (brown) reflect reductions in ice-phase condensate.

spatial distribution likely reflects the differing injection locations and associated storm dynamics. Notably, Δq_c reaches the highest altitudes—up to 10 km—in both the total and periphery experiments, indicating vigorous vertical transport of cloud water into the mid- to upper troposphere. By 18:00 UTC, positive Δq_c values persist in all cases, although the anomalies appear more radially and vertically dispersed and are partially accompanied by minor negative differences. The overall magnitude of the anomaly is lower compared to the earlier time step, suggesting a potential weakening of the seeding effect over time. It is important to emphasize, however, that the absolute differences in q_c remain relatively small—generally below 0.0002 kg/kg. Although the seeding induces spatially organized changes in cloud water distribution, the limited magnitude of these anomalies may explain the absence of substantial alterations to the overall storm structure.

Cloud Ice Content (Δq_i): The changes in cloud ice content largely mirror those observed in Δq_c . In the eyewall seeding case, the response is minimal, with only a slight reduction in q_i near the upper portions of the eyewall and a marginal increase in the upper outflow region. This indicates limited vertical redistribution of ice-phase condensate as a result of the seeding. In contrast, the total and periphery seeding experiments show a clearer response 24 hours after seeding. Both cases exhibit a decrease in q_i near the upper eyewall region, along with a slight increase within the eye, possibly indicating a shift in vertical ice distribution or suppressed glaciation in the convective core. These anomalies, however, diminish significantly by +36 hours and, in the case of the periphery experiment (2e6p), even reverse—suggesting a transient and spatially variable microphysical response. Overall, the relatively small magnitudes of Δq_i suggest that any seeding-induced modulation of glaciation processes is subtle and likely short-lived, with more substantial effects limited to specific storm regions and time periods.

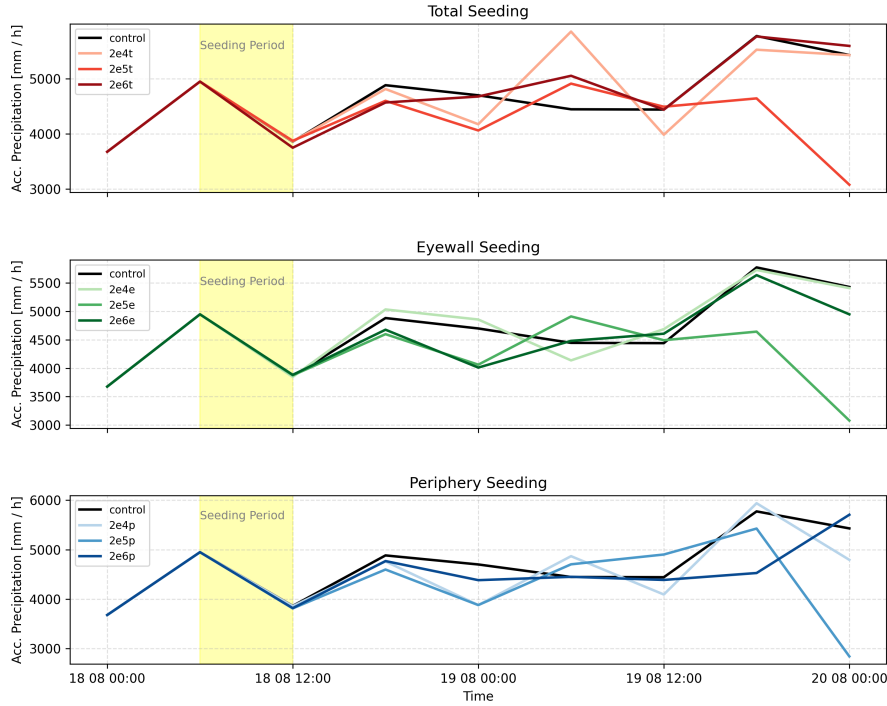


Figure 12: Precipitation time series for all CCN seeding experiments. Each panel shows the accumulated precipitation in each timestep with a radius of 500 km, for a different seeding region: Total Seeding (top), Eyewall Seeding (middle), and Periphery Seeding (bottom). Colored lines represent different CCN concentrations, while the black line shows the unperturbed control simulation. The light yellow shaded area marks the 6-hour seeding period on 18 August 2005 from 06:00 to 12:00 UTC.

3.6 Precipitation

Figure 12 The figure provides an overview of both the temporal evolution and total amount of accumulated precipitation for all seeding experiments and the control run. Across all simulations, the general precipitation pattern is characterized by an initial peak, followed by a dip, a gradual decline, and a final maximum around landfall on 19 August at 18:00 UTC. Seeded simulations begin to diverge from the control shortly after the seeding window (marked in yellow). A recurring pattern in several experiments—most notably in cases 2e4t, 2e5e, and 2e5p—is a pronounced drop in precipitation accumulation 12 hours after seeding, followed by an overshoot 6 to 12 hours later over control levels. This dip-and-rebound behavior mirrors what is observed in other intensity metrics, such as minimum sea level pressure and maximum wind speed. Interestingly, case 2e6p is the only scenario where total precipitation

remains consistently below that of the control. The notable precipitation drops in the 2e5(t,e, p) cases can be traced back to inconsistencies in TC center identification by the tracking algorithm, which led to mismatches in the spatial domain considered during extraction.

Figure 13 shows snapshots of the instantaneous precipitation rate (mm/h) at +24 h and +36 h after seeding for the control simulation and the three seeding experiments (total, eyewall, and periphery). All panels represent storm-centered domains and correspond to ICON output at 06:00 UTC and 18:00 UTC on 19 August 2005, respectively.

In the control simulation, precipitation exhibits a broadly symmetric structure with peak intensities surrounding the eyewall. The total seeding experiment shows slightly enhanced rainfall at +24 h, accompanied by a more compact precipitation structure near the eyewall and a reduction in rainband activity by +36 h. The eyewall seeding case produces intense rainfall confined to the storm core at +24 h, while outer rainbands are nearly absent. By +36 h, the precipitation structure appears more disorganized near landfall, with a fragmented eyewall. The periphery experiment displays the most disorganized and spatially scattered rainfall pattern at +24 h, but gains some structural organization again at +36 h.

These results suggest that CCN injections into different storm regions affect the spatial distribution and organization of precipitation in distinct ways. While no consistent trend emerges across all cases, the eyewall seeding scenario leads to strong localized enhancement early on, whereas periphery seeding tends to suppress and fragment precipitation, particularly in the outer storm regions.

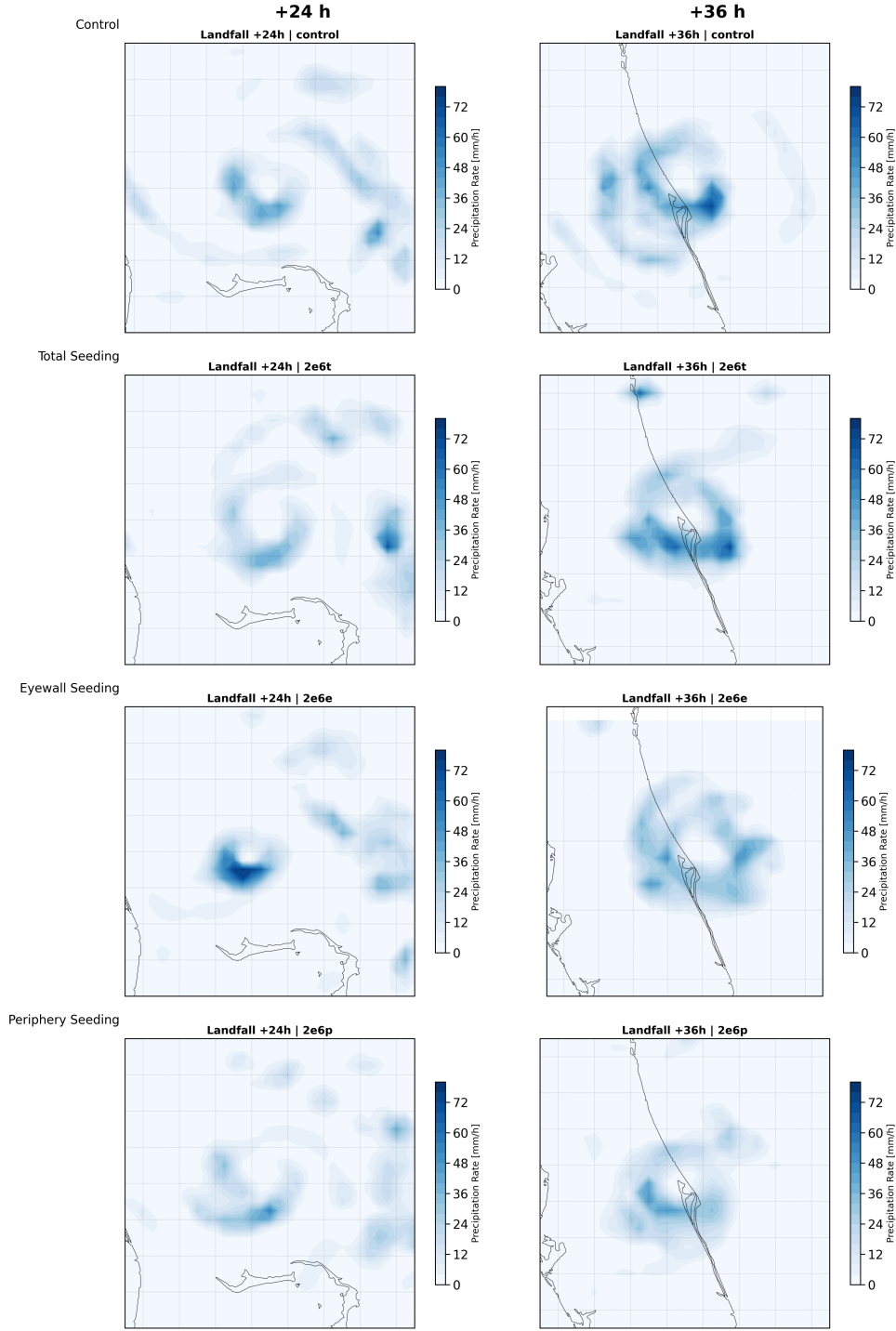


Figure 13: Snapshots of instantaneous precipitation rate (mm/h) from the ICON model output at +24 h (left) and +36 h (right) after seeding. Rows correspond to the control run and three seeding configurations: total, eyewall, and periphery. Each panel shows the storm-centered precipitation field within the model domain.

3.7 Thermodynamics

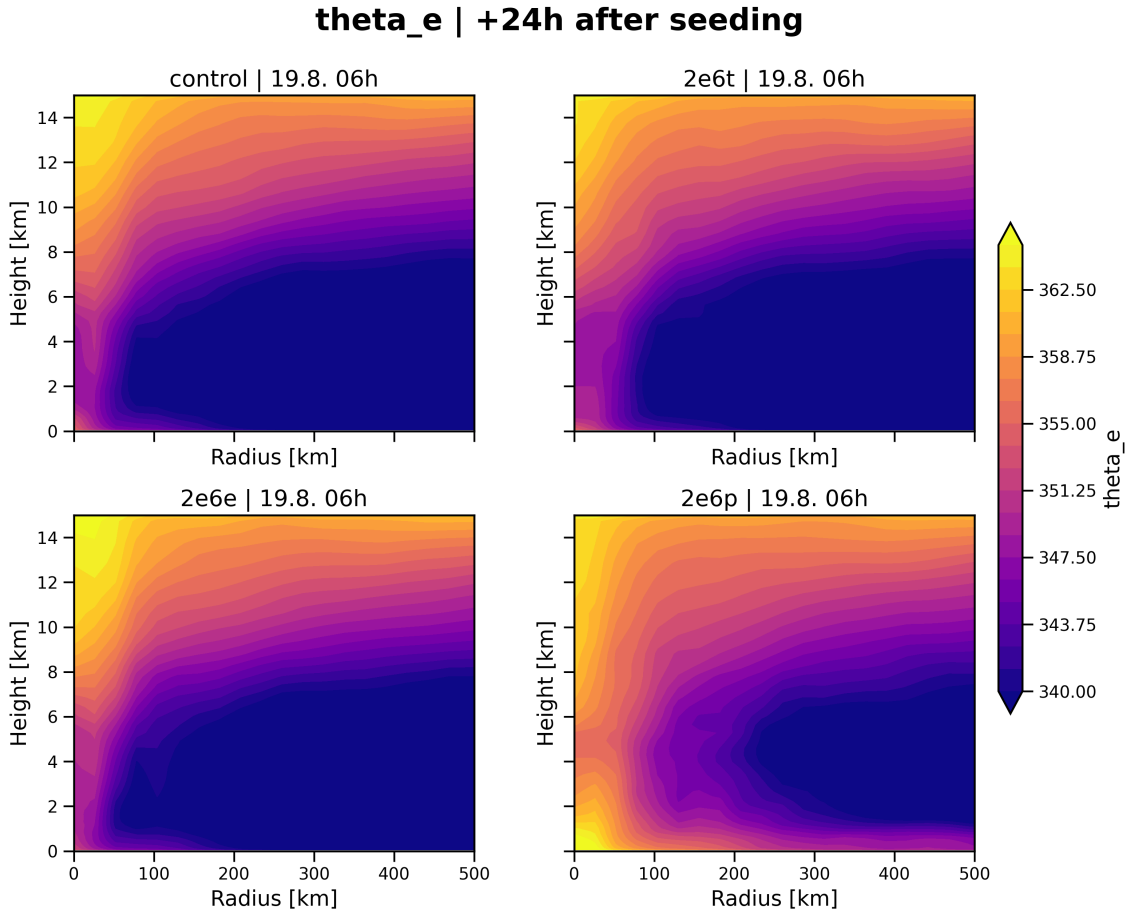


Figure 14: Azimuthally averaged equivalent potential temperature (θ_e) at 06:00 UTC on 19 August 2005, i.e. 24 hours after the start of seeding.

To assess the thermodynamic evolution of the storm and the effect of aerosol perturbations on deep convective potential, the equivalent potential temperature (θ_e) was analyzed in radial-vertical cross sections. Since θ_e integrates both sensible and latent heat, it serves as a robust proxy for moist static energy and convective instability. In general, an increase in θ_e indicates a warmer and/or moister atmosphere, while a decrease suggests drying or cooling.

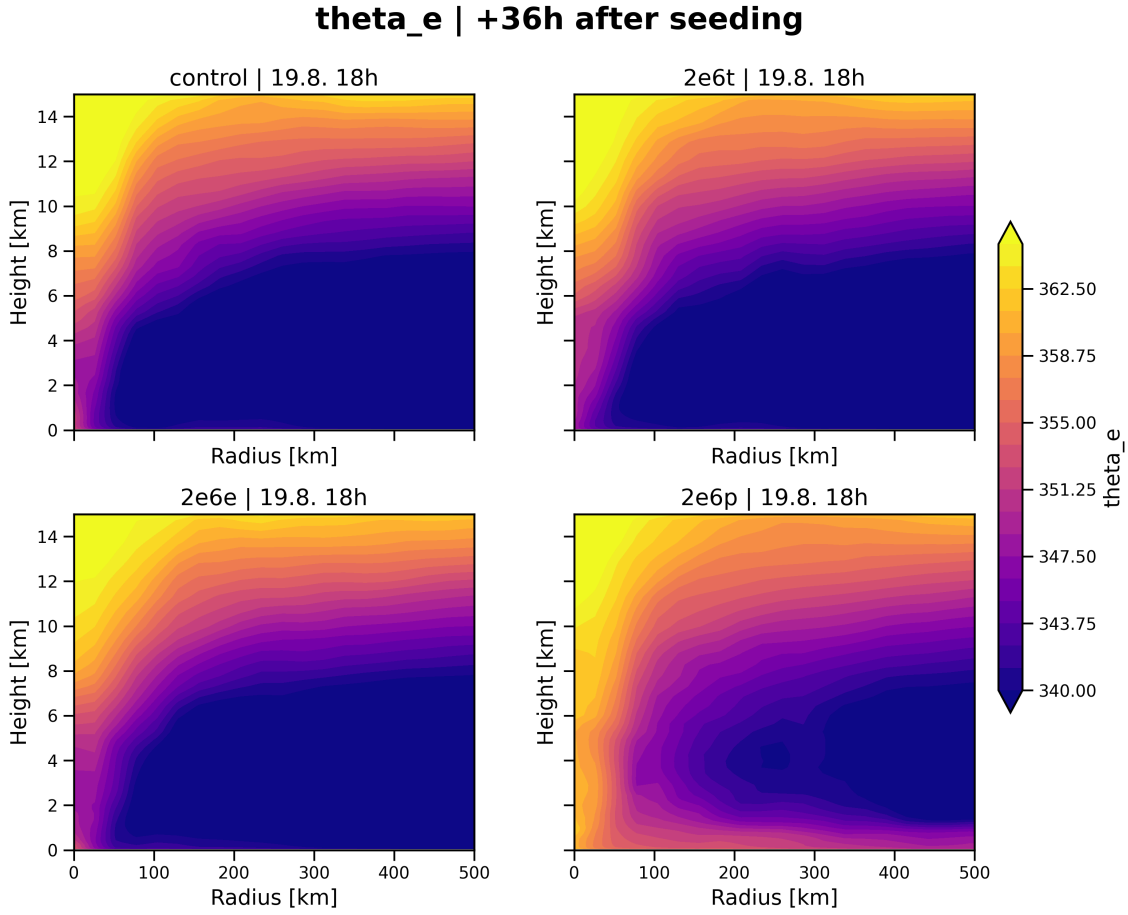


Figure 15: Same as Figure 14, but for 18:00 UTC on 19 August 2005 (i.e. +36h after seeding).

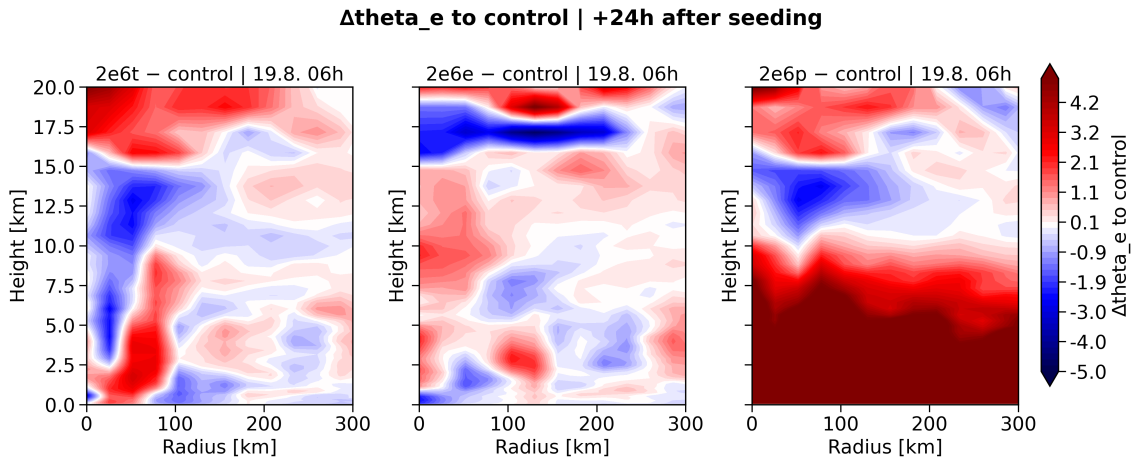


Figure 16: Difference in equivalent potential temperature (θ_e) between each high-intensity seeding experiment (2e6t, 2e6e, 2e6p) and the control simulation at 06:00 UTC on 19 August 2005 (+24h after seeding). Positive values (red) indicate warmer and/or moister air masses compared to control.

Thermodynamic response – equivalent potential temperature (θ_e):

A first look at the absolute θ_e fields (Figures 14 and 15) reveals a distinct thermodynamic modification in experiment 2e6p. Compared to the control, θ_e values are notably elevated, and the contour lines extend radially outward, indicating an expanded region of enhanced moist static energy. This suggests that periphery seeding creates a more favorable thermodynamic environment, not only within the storm core but also across the outer rainbands.

Interestingly, a weak discontinuity emerges in the mid-troposphere of 2e6p, possibly indicative of inhibited vertical mixing or localized stratification. The total seeding case (2e6t) also shows enhanced θ_e , albeit with a weaker signal, while the eyewall seeding experiment (2e6e) remains largely similar to the control in both magnitude and structure.

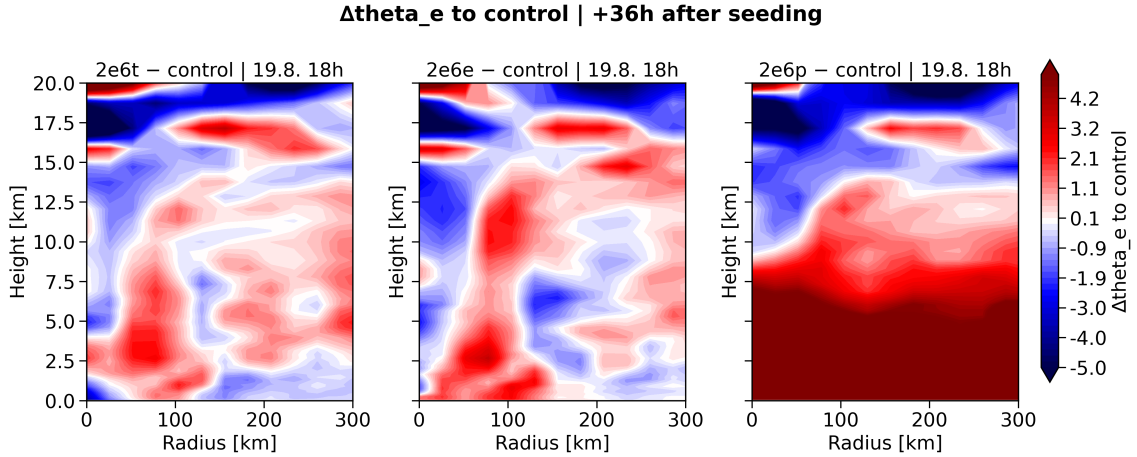


Figure 17: Same as Figure 16, but for 18:00 UTC on 19 August 2005 (+36h after seeding).

At +24h post seeding (Figure 16), distinct spatial patterns in the differential image emerge:

- In the total seeding experiment (2e6t), a decrease in θ_e is observed near the storm center (0–50km), followed by a secondary maximum around 100km radius. This suggests a radial shift of the eyewall and a redistribution of moist static energy toward the outer core.

- The eyewall case (2e6e) shows only minor deviations from control. A modest increase in θ_e is present throughout the lower and mid-troposphere, while a cooling layer appears around 17.5km, likely due to enhanced detrainment or reduced overshooting convection.
- The periphery case (2e6p) exhibits the strongest thermodynamic signal. Almost the entire troposphere below 10km shows a coherent increase in θ_e of more than 4K, pointing to significant moisture accumulation. This indicates modified cloud microphysics in outer rainbands, where suppressed warm-rain processes lead to delayed precipitation and increased vapor retention in the boundary layer.

By +36h (Figure 17), these tendencies persist and intensify in the periphery seeding case. The enhancement of θ_e expands vertically, covering nearly the full tropospheric depth. However, a strong cooling signature emerges in the upper troposphere. The other two experiments show mixed signals: alternating bands of warming and cooling. Notably, a warm ring emerges outside the control’s eyewall in both 2e6t and 2e6e, which may point to an outward shift of convective activity and could be a precursor to an eyewall replacement cycle.

In summary, the strongest and most coherent thermodynamic modification occurs in the periphery seeding experiment. The sustained elevation of θ_e across 24–36 hours suggests a robust and persistent microphysical response that modifies the storm’s energetics. While central seeding induces only subtle changes, peripheral injections appear capable of reshaping the storm’s secondary circulation and thermodynamic structure—supporting the hypothesis that cloud microphysical perturbations can exert large-scale impacts on TC environments.

3.8 Wind Fields

For a final insight into the data this section will have a look into the changes of the circulation patterns of the TC. While the primary circulation is characterized by the tangential winds (winds around the TC). The secondary circulation is characterized by the radial wind (inflow and outflow) and the vertical velocities (ascent in the eyewall).

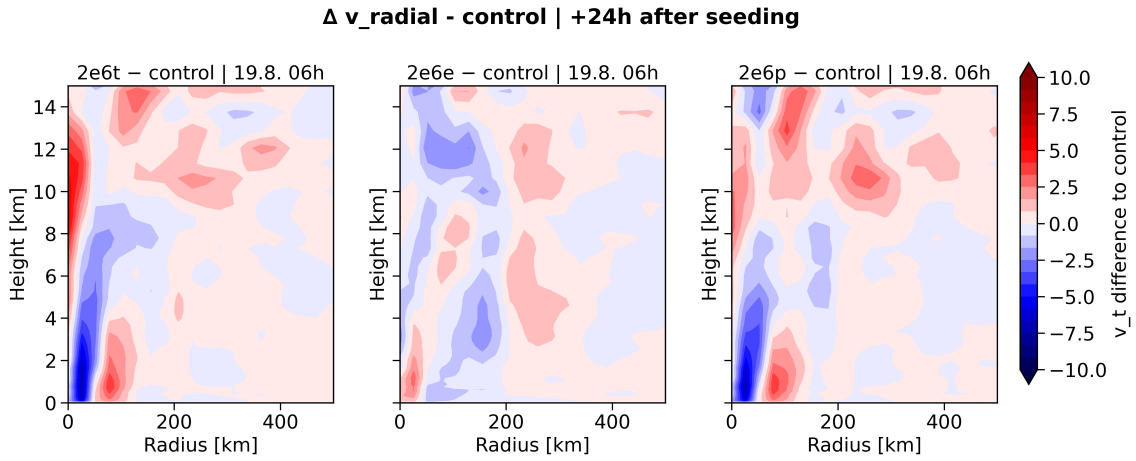


Figure 18: Azimuthally averaged differences in tangential wind speed (v_t) between the three high-intensity seeding experiments (2e6t, 2e6e, and 2e6p) and the control simulation at 06:00 UTC on 19 August 2005. Differences are shown as radius–height cross-sections, with positive values (red) indicating enhanced cyclonic motion and negative values (blue) indicating a weakening relative to the control. This time step corresponds to the storm’s peak intensity at landfall.

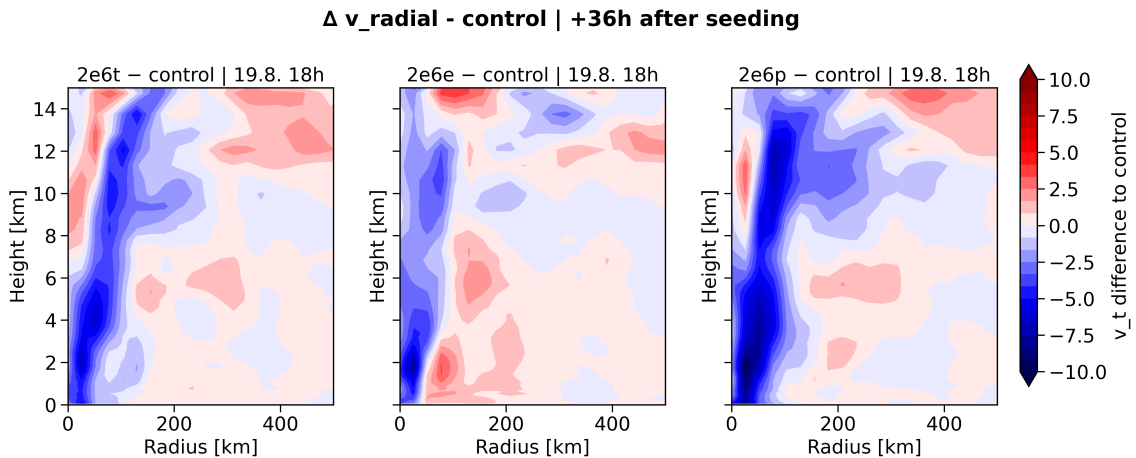


Figure 19: Same setting as in Figure 18, but for 18:00 UTC on 19 August—twelve hours later, at landfall.

Tangential velocities

Similar to the changes observed in vertical velocity, the tangential wind field also responds to CCN perturbations. Initially, the response is minor—particularly in the 2e6e case, where structural changes in the eyewall remain negligible even 24 hours after seeding initiations. In all experiments, the eyewall appears slightly weaker than in the control, yet small increases in wind speed emerge approximately 30 km outside the inner core. This may suggest a broader eyewall compared to the control.

By landfall (+36 h), the differences become more pronounced. Across the entire eyewall column, tangential wind speeds are reduced by up to 10 m s^{-1} . The strongest weakening occurs in the periphery-seeded experiment (2e6p), particularly within the outflow and upper-level regions outside the eyewall. In contrast, the eyewall-seeded case (2e6e) exhibits only minor reductions while again hinting at a broader core structure.

These patterns indicate that aerosol injections—especially into the storm’s outer regions—can influence not only localized convection but also the broader azimuthal momentum distribution, i.e., the storm’s primary circulation. While no strategy leads to a drastic disruption of the cyclone’s overall rotation at peak intensity, inner-core anomalies suggest short-lived structural shifts that could affect storm intensity in the hours following seeding.

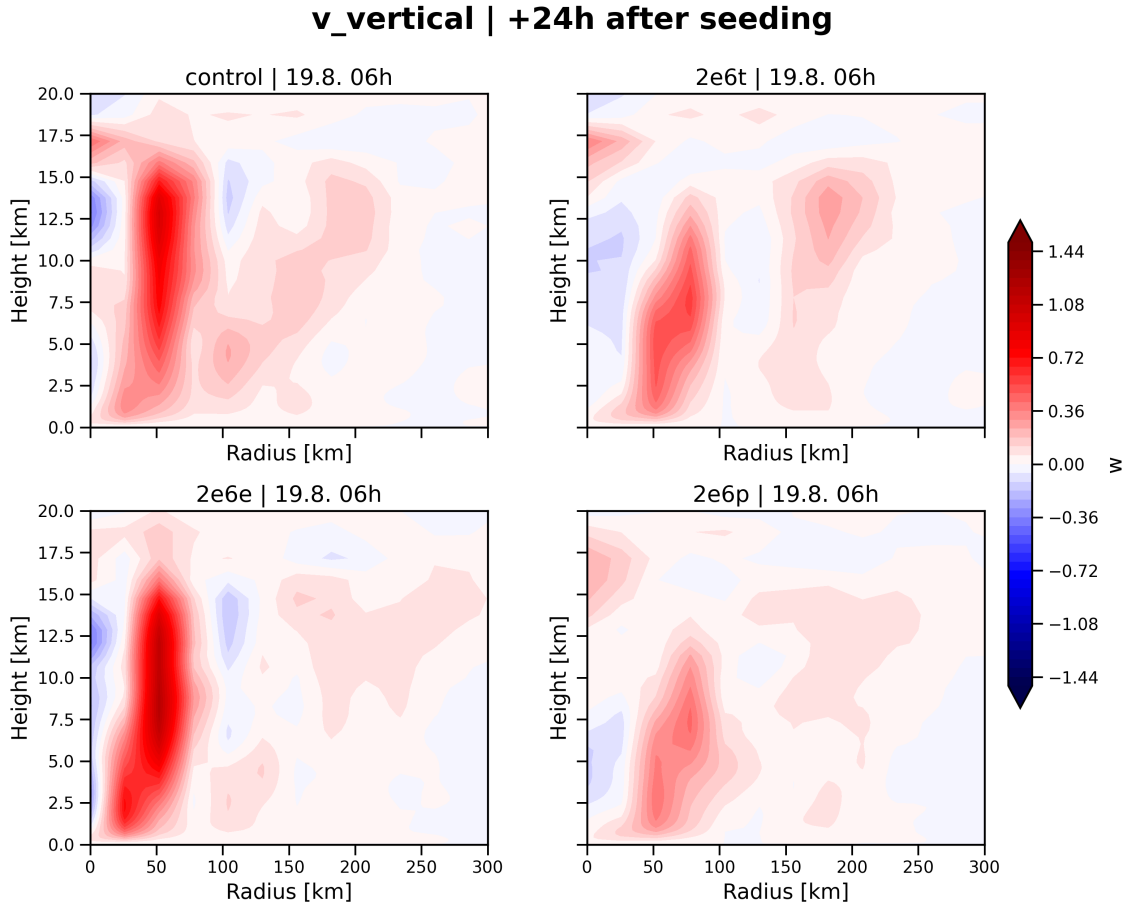


Figure 20: Radius–height cross-sections of vertical velocity (w) for the control and 2e6 seeding experiments (total, eyewall, periphery) on 19 August 2005 at 06:00 UTC. The panels show azimuthally averaged vertical motions within 300 km of the storm center, calculated in ring bands of 26 km width. Updrafts and downdrafts are represented by positive and negative values, respectively. The comparison illustrates differences in the vertical structure of convection associated with the respective seeding strategies.

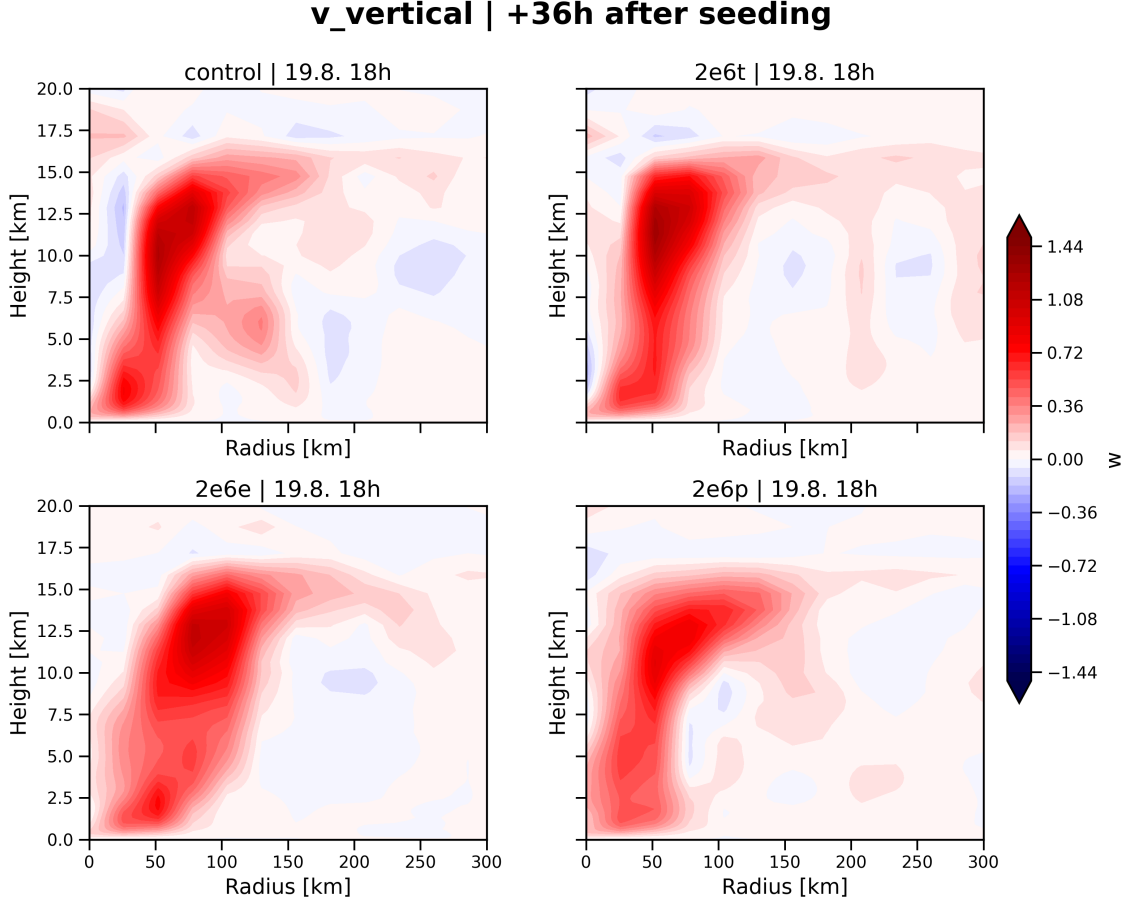


Figure 21: Same setting as in Figure 20, but for the time step 12 hours later — August 19 at 18:00 UTC.

Vertical velocities Figures 20 and 21 display vertical cross-sections of the azimuthally averaged vertical velocity w for the control simulation and the three high-intensity seeding experiments with a CCN injection scenario of $2 \times 10^6 \text{ cm}^{-3} \text{ s}^{-1}$ (2e6t, 2e6e, and 2e6p). The first time step (19 August, 06:00 UTC) corresponds to the time of strongest signal in sea level pressure and maximum wind speed anomalies (cf. Section 3.6), while the second (19 August, 18:00 UTC) represents the time of maximum storm intensity (63 m s^{-1} ; 946.93 hPa), coinciding with Category 4 landfall (cf. Section 3.1).

Although the maximum vertical velocity of approximately 1.2 m s^{-1} in the control case may appear modest, it is important to note that these values are azimuthally averaged over ring bands. In cases where the eyewall is not perfectly axisymmetric,

these averages may underestimate localized peaks and distort the actual convective intensity.

Compared to the control run, only the eyewall seeding case (2e6e) retains a similar structure and peak vertical velocity. In fact, it exhibits a broader and more vigorous updraft between 5 and 15 km altitude. In contrast, both the periphery (2e6p) and total (2e6t) seeding scenarios show weaker and more disorganized vertical motion within the eyewall, alongside a broader region of diffuse ascent farther from the storm center. This suggests a redistribution of convection from the inner core toward the outer rainbands. Notably, downdrafts in the TC center are observed only in the control and eyewall seeding cases.

As also seen in the precipitation fields (Section 3.6), the convective structure of the eyewall recovers in all simulations between 06:00 and 18:00 UTC. Vertical velocities increase in all cases, with the control simulation reaching $w_{\max} \approx 1.2 \text{ m s}^{-1}$ and the seeding cases up to $w_{\max} \approx 1.5 \text{ m s}^{-1}$ (e.g., in 2e6t). This could indicate a temporary invigoration of convection due to enhanced CCN concentrations, particularly in the inner-core region. The radial differences in updraft structure further highlight that the injection location may critically influence the spatial organization of the storm —without necessarily altering peak storm intensity significantly.

Overall, the structure and magnitude of vertical motions in the eyewall region diverge significantly shortly after the seeding phase, but tend to return to near-control characteristics by the time of landfall.

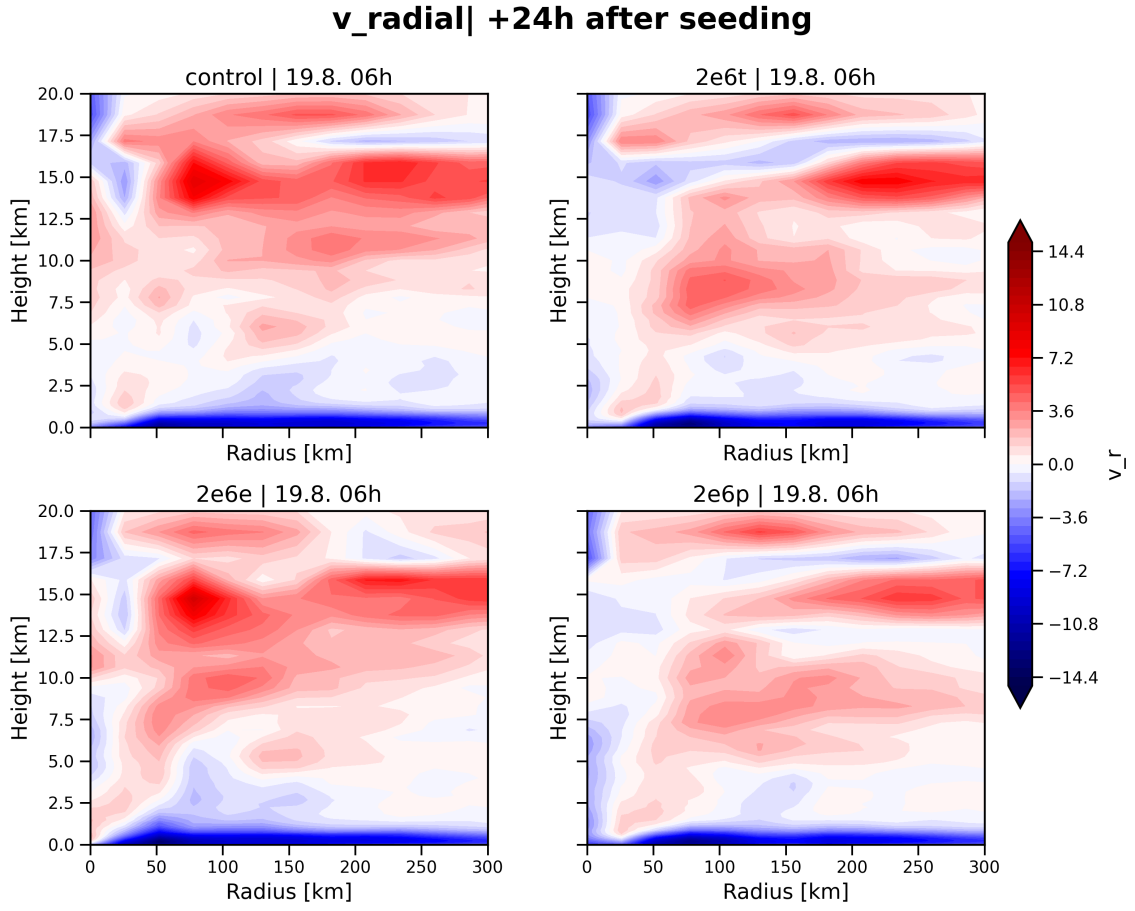


Figure 22: Azimuthally averaged radial wind speeds (v_r) at 06:00 UTC on 19 August 2005, 24 hours after the onset of seeding. Positive values (red) indicate outflow, negative values (blue) indicate inflow. Shown are four experiments: control, 2e6t (total seeding), 2e6e (eyewall seeding), and 2e6p (periphery seeding).

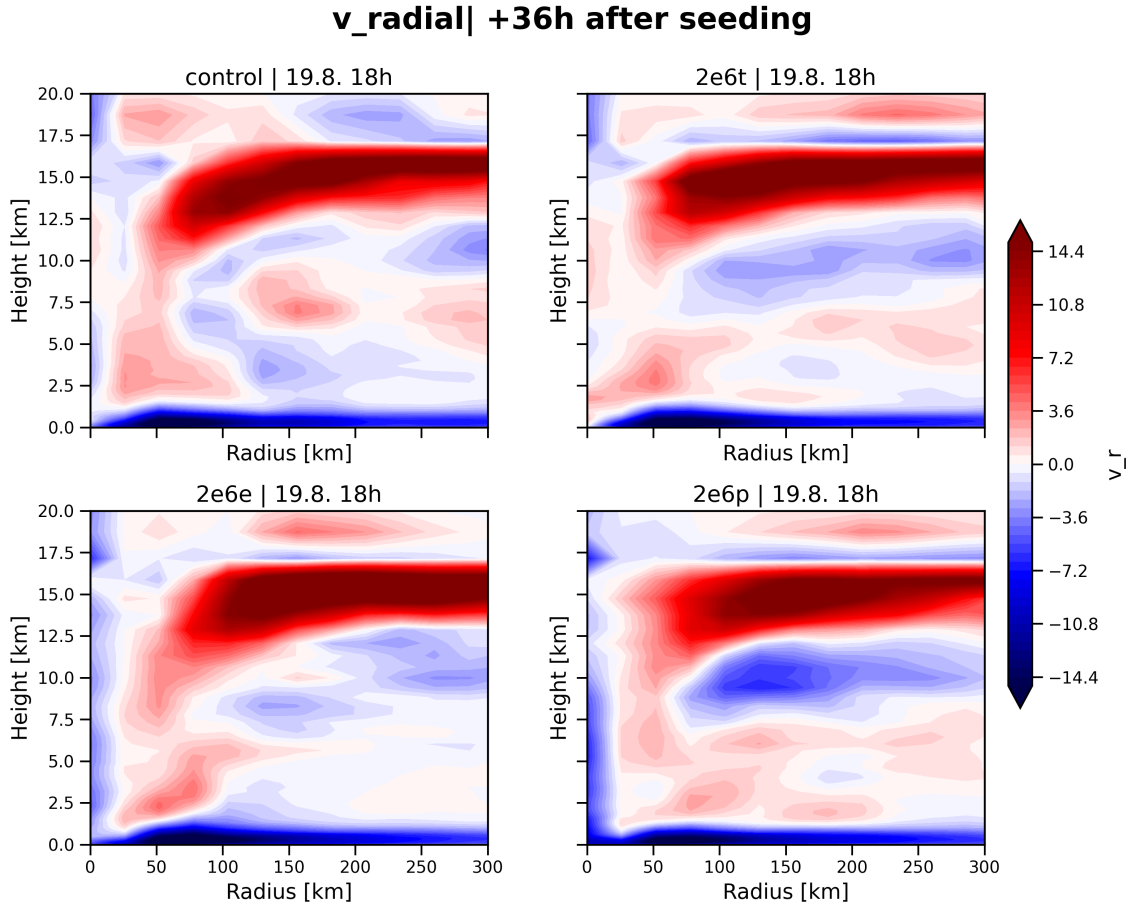


Figure 23: Same setting as in Figure 22, but for 18:00 UTC on 19 August—36 hours after seeding.

Radial velocities In the radial velocities the patterns of each experiment as well as both time steps of Figures 22 and 23 do not show as structural differences to the control case as they do in the previously shown wind components. Figure 23 shows an overall strong secondary circulation. While inflow-value levels stay approximately the same the upper-level outflow becomes more pronounced in all experiments, especially in 2e6p and 2e6e. The most notable difference though is in that all experiments show inhibited mid-troposphere inflow especially in the periphery case (2e6p), where strong inflow in the lower and mid-troposphere coincides with enhanced outflow aloft, indicating a vertically coherent secondary circulation response to seeding. The case in 2e6p also shows some lower troposphere outflow at around 2km, which does not occur in the control case.

3.9 Summary of Results

The conducted sensitivity experiments reveal a nuanced picture of how TCs respond to artificial CCN seeding under varying spatial configurations. While individual variables display local anomalies, the overall structure and evolution of the cyclone remain remarkably robust—particularly in the short term and in the control-like recovery phases.

From a dynamical perspective, the seeding effects are most visible in the early stages following injection, with total and periphery seeding producing the clearest signals. The total seeding experiment (2e6t) results in a brief overshoot of intensity, reaching Category 5 with maximum wind speeds surpassing the control simulation. However, this peak is short-lived and not accompanied by a corresponding deepening of the central pressure. In contrast, periphery seeding (2e6p) causes a more pronounced—but temporary—weakening of the storm, visible in both wind speed and sea-level pressure. All cyclones eventually converge toward control-like intensity prior to landfall, and no lasting structural disruption occurs. Eyewall seeding shows the weakest influence overall, with most variables displaying only minimal deviations from the control.

The cloud microphysical response, as seen in changes to cloud liquid water (q_c) and cloud ice content (q_i), is spatially heterogeneous and relatively modest in magnitude. Increases in q_c are observed in all experiments shortly after seeding, with maxima typically located in the eyewall and outer rainbands. These anomalies are most pronounced in the total and periphery cases, where cloud water reaches altitudes of up to 10 km, suggesting enhanced vertical transport. However, the overall differences remain small—below 0.0002 kg/kg—and decay over time. The q_i field shows weak and transient reductions in the upper eyewall, especially in the periphery and total seeding experiments, possibly reflecting a suppression of glaciation or altered vertical redistribution of condensate.

The thermodynamic response, assessed via equivalent potential temperature (θ_e),

highlights the most consistent and spatially coherent anomaly. In the periphery experiment, a marked increase in θ_e of up to 4 K extends across the lower and mid-troposphere, implying enhanced moist static energy and moisture retention. This thermodynamic signal persists and intensifies over time, whereas the other two cases exhibit more subtle and patchy deviations.

Changes in the wind field provide further support for the differentiated impact of seeding strategies. Tangential wind speed weakens slightly in all cases, particularly in the outer core regions, with the most distinct reduction seen in the periphery experiment. Vertical velocity fields indicate that convection becomes more disorganized and distributed in total and periphery seeding, while the eyewall case retains a concentrated and symmetric updraft structure. The radial wind response suggests a more coherent secondary circulation in the periphery case, with enhanced inflow in the lower and mid-troposphere and stronger outflow aloft.

In summary, the experiments demonstrate that CCN seeding can introduce localized and time-limited changes to TC structure and dynamics. The extent and persistence of these changes depend strongly on the injection location. While central seeding produces immediate but transient effects, periphery seeding leads to more persistent thermodynamic and kinematic adjustments—albeit without fundamentally altering the cyclone’s trajectory or long-term intensity. These findings support the hypothesis that cloud microphysical perturbations can influence storm processes, but also highlight the resilience of mature TCs to external aerosol forcing.

4 Discussion and Conclusion

4.1 Comparison with the Literature

The results of the ICON simulations broadly support the theoretical expectations derived from earlier studies, while also revealing spatial and temporal differences in the magnitude and persistence of the observed effects.

Peripheral Seeding - Suppression of Inner-Core Convection: Several studies (e.g., Khain et al., 2008; Rosenfeld et al., 2007; Zhang et al., 2007) propose that CCN injections into outer rainbands invigorate convection there, thereby diverting moisture flux away from the eyewall and weakening inner-core convection.

Observation: The periphery experiments—particularly 2e6p—demonstrate:

- a weakening and radial broadening of updrafts within the core region,
- a distinct increase in equivalent potential temperature (θ_e) across the outer storm (up to +4 K),
- and a redistribution of latent heat away from the eyewall.

This aligns well with theoretical expectations and indicates that outer-region seeding can reshape the storm’s thermodynamic and dynamical structure.

Eyewall Seeding - Updraft Invigoration via Delayed Precipitation According to Lee et al., 2024; Rosenfeld et al., 2012, CCN introduced into the eyewall inhibit warm rain processes, allowing more supercooled water to ascend and release latent heat upon freezing, thereby strengthening updrafts.

Observation: Experiment 2e6e shows:

- more vertically coherent and intense updrafts in the eyewall,
- but minimal changes in θ_e , pressure, or maximum wind speed.

This suggests that although localized invigoration occurs, it is not sufficient to modify the storm’s overall intensity or structure in the absence of favorable environmental conditions.

Total Seeding: Nonlinear and Mixed Feedbacks Literature such as Liang et al., 2021 highlights that seeding across all radial zones can trigger competing feedbacks between the inner and outer core, leading to ambiguous net outcomes.

Observation: The total seeding experiment 2e6t exhibits:

- a temporary overshoot in wind speed (Category 5, 70.5 m/s),
- no corresponding pressure deepening or lasting intensification,
- a dip in θ_e near the center, but a ring-shaped enhancement at 100–150 km radius, possibly linked to a radial eyewall shift.

These patterns are indicative of short-lived, nonlinear responses rather than deterministic restructuring.

Precipitation: Delayed Onset and Spatial Redistribution Several studies (e.g., rosenfeld2012aerosol; zhao2018enlarging) describe how CCN seeding can suppress warm rain formation, delay precipitation onset, and shift rainfall to outer regions.

Observation: Many experiments (e.g., 2e5e, 2e5p) show:

- a dip-rebound pattern in precipitation within 12–24 hours post-seeding,
- and in case 2e6p, a persistently lower total precipitation compared to control.

This supports the notion of reduced autoconversion and delayed rainfall linked to aerosol perturbations.

Storm Track - No Significant Alteration Earlier modeling studies Jiang et al., 2016; Lin et al., 2011 report no consistent evidence of aerosol-induced track deviations.

Observation: In all simulations, storm tracks remain nearly identical, with land-fall locations within a ~ 100 km coastal band. This confirms that CCN seeding does not significantly alter TC trajectory under the given experimental setup.

Summary Overall, the ICON experiments qualitatively reproduce several literature-based expectations:

- Peripheral seeding weakens the core and enhances outer convection,
- Eyewall seeding strengthens updrafts but without dynamical intensification,
- Total seeding produces mixed and nonlinear responses.

However, none of the strategies resulted in sustained or large-scale restructuring of the cyclone. The results emphasize both the sensitivity and the resilience of TC to microphysical perturbations. Future ensemble modeling is essential to constrain uncertainties and assess robustness.

4.2 Limitations

4.2.1 Model Noise and Structural Uncertainty

Although most the findings in this study align with the literature there are limitations to this study. The simulation setup, while high-resolution and physically consistent, remains prone to inherent model noise and internal variability. Several metrics—especially vertical wind speed and precipitation—show considerable fluctuations even in the control simulation. These stochastic elements likely stem from turbulent convection, non-linear feedbacks, and the chaotic nature of moist atmospheric processes (i.e. Butterflyeffect) (Lorenz, 1963) . Moreover, some responses (e.g., mid-tropospheric cooling or anomalous secondary inflows) may reflect

structural uncertainties amplified by minor perturbations rather than deterministic physical responses. This interpretation is supported by the spatial patchiness of Δq_i and the temporal inconsistency in precipitation changes.

4.2.2 Limitations related to Model Performance

Although the model integration time step was set to 50 seconds, output fields were only saved at six-hour intervals. This temporal resolution significantly limits the ability to resolve rapid transitions in T intensity and structure. In the case studied here, the cyclone underwent a rapid intensification from Category 1 to Category 4 within just 48 hours—an evolution that likely involved short-lived but dynamically important processes not captured in the available output.

Furthermore, the TC tracking algorithm failed to correctly identify the storm center in several of the 2e5 experiments after seeding. As a result, key intensity metrics such as maximum wind speed and minimum sea level pressure were mislocated or omitted during the most active phases. This compromised the interpretation of the seeding response in these cases and highlights the need for either higher-frequency output or more robust storm-tracking methods in future simulations.

4.3 On the Idealized Nature of the Seeding Setup

It is important to emphasize that the aerosol seeding scenarios employed in this study are purely idealized and should not be interpreted as operationally feasible interventions. Both the magnitudes of the injected CCN concentrations (up to $2 \times 10^6 \text{ cm}^{-3} \text{ s}^{-1}$) and the spatial extent of the seeding regions (covering hundreds of kilometers) far exceed what is currently achievable with real-world cloud seeding technologies. Even assuming perfect dispersion, the logistical, technological, and atmospheric challenges of delivering such particle loads into a mature TC are immense.

Moreover, the seeding was performed instantaneously and uniformly over fixed

domains, neglecting the complexities of aerosol transport, scavenging, and activation in real atmospheric conditions. The assumed CCN properties (e.g., size, solubility, composition) were simplified and held constant across all experiments.

These constraints underline that this study represents a model-based sensitivity analysis—not an operational proposal. Its aim is to isolate physical mechanisms and evaluate the plausibility of storm modulation in a controlled numerical environment. Translating such effects into reality would require fundamentally different experimental designs, technological capabilities, and ethical considerations.

4.3.1 Limitations due to Missing Ensemble Simulations

A major limitation of this study is the lack of ensemble simulations. All results are based on single realizations per experiment, making it difficult to robustly quantify uncertainty or distinguish deterministic responses from random variability. Given the strong sensitivity of TC dynamics to initial conditions and the stochastic nature of convection, ensemble approaches would be essential to:

- assess the statistical significance of observed responses,
- evaluate the spread of possible outcomes under identical seeding scenarios,
- and provide confidence intervals for structural variables such as wind fields and θ_e .

Without ensemble simulations, the presented results should be interpreted as indicative trends rather than definitive outcomes.

4.4 Relevance and Implications

Despite these limitations, the findings provide valuable insight into how spatially targeted CCN injections affect TC structure. The fact that periphery seeding can produce coherent thermodynamic anomalies and redistribute convective energy confirms the theoretical potential for aerosol-based storm modulation. However, the

storm’s resilience—manifested in its recovery toward control-like intensity before landfall—highlights the limits of single-seeding strategies. Future work should combine ensemble modeling with realistic seeding scenarios, including varying aerosol compositions and ocean–atmosphere coupling. These efforts are necessary not only for advancing the scientific basis of geoengineering, but also for improving our understanding of aerosol–convection interactions in extreme weather systems.

4.5 Conclusion and Outlook

This study demonstrates that the spatial configuration of aerosol seeding exerts a first-order control on the dynamical and thermodynamical response of TCs. While peripheral CCN injections can suppress core intensity by redistributing moist static energy, central seeding primarily alters vertical dynamics without leading to systemic changes. Despite the high-resolution model setup, structural limitations and the lack of ensemble simulations prevent firm conclusions about long-term storm modulation potential.

Nonetheless, the presented results strengthen the physical basis for aerosol–convection interaction studies and highlight the need for future ensemble-based, multi-model investigations that consider environmental variability and coupling with oceanic processes. Ultimately, this work contributes to the scientific foundation needed for critical evaluation of geoengineering strategies in the context of TC risk reduction.

4.6 Recommendations for Future Research

Building upon the findings and limitations of this study, several research avenues are recommended to further advance the understanding of aerosol-TC interactions:

- **Ensemble simulations:** Given the strong sensitivity of TC evolution to initial conditions and the inherent chaotic dynamics of moist convection, ensemble-based approaches are essential. They would allow for a robust quantification

of uncertainty and help distinguish systematic responses from stochastic variability.

- **Higher temporal output resolution:** Saving model fields at higher frequency (e.g., hourly or sub-hourly) would enable a more detailed analysis of rapid intensification phases and transient feedback mechanisms that were not resolved in the current six-hourly output.
- **Ocean–atmosphere coupling:** Including interactive sea surface temperatures (SST) and ocean feedbacks could substantially alter the TC response to CCN forcing, especially for prolonged simulations or landfall scenarios.
- **Microphysical sensitivity tests:** A systematic comparison of different cloud microphysics schemes (e.g., single-moment vs. multi-moment, bin schemes) would help isolate scheme-specific responses and improve the generalizability of the results.
- **Realistic aerosol initialization:** Incorporating observationally constrained CCN concentrations (e.g., from MODIS, AERONET, or in-situ aircraft data) would enable scenario simulations that better reflect real-world variability and aerosol mixtures (e.g., sea salt, dust, combustion particles).
- **Satellite and radar validation:** Future studies should compare model output with high-resolution satellite and radar observations (e.g., TRMM, GPM, CloudSat) to evaluate how well seeding impacts manifest in observable variables such as reflectivity, rain rate, or cloud top height.
- **Exploration of seeding strategies:** Beyond fixed spatial seeding zones, adaptive or mobile seeding strategies (e.g., targeting developing convective bursts) could be investigated to assess whether more effective modulation outcomes can be achieved under realistic constraints.

These extensions would not only increase confidence in the simulation results but also enhance their relevance for geoengineering assessments and disaster risk reduction strategies in cyclone-prone regions.

References

- Arieli, Y., Khain, A., Gavze, E., Altaratz, O., Eytan, E., & Koren, I. (2025). The impact of cumulus clouds and CCN regeneration on aerosol vertical distribution and size. *Journal of the Atmospheric Sciences*, 82(1), 107–118. <https://doi.org/10.1175/JAS-D-24-0112.1>
- Beven, J. L., Stewart, S. R., Lawrence, M. B., Avila, L. A., Franklin, J. L., & Pasch, R. J. (2008). ANNUAL SUMMARY: Atlantic hurricane season of 2005 [Publisher: American Meteorological Society]. *Monthly Weather Review*, 131(7), 1454–1484. [https://doi.org/10.1175/1520-0493\(2003\)131<1454:ashso>2.0.co;2](https://doi.org/10.1175/1520-0493(2003)131<1454:ashso>2.0.co;2)
- Carrio, G. G., & Cotton, W. R. (2011). Investigations of aerosol impacts on hurricanes: Virtual seeding flights. *Atmospheric Chemistry and Physics*, 11(6), 2557–2567. <https://doi.org/10.5194/acp-11-2557-2011>
- Chan, K. (2023). Evaluating potential impact of seeding tropical cyclones with aerosols in the numerical model ICON.
- Emanuel, K. A. (1986). An air-sea interaction theory for tropical cyclones. part i: Steady-state maintenance. *Journal of the Atmospheric Sciences*, 43(6), 585–604. [https://doi.org/https://doi.org/10.1175/1520-0469\(1986\)043<0585:AASITF>2.0.CO;2](https://doi.org/https://doi.org/10.1175/1520-0469(1986)043<0585:AASITF>2.0.CO;2)
- Emanuel, K. A. (1994). *Atmospheric convection*. Oxford University Press.
- Enz, B. M., Engelmann, J. P., & Lohmann, U. (2023). Use of threshold parameter variation for tropical cyclone tracking. *Geoscientific Model Development*, 16(17), 5093–5112. <https://doi.org/10.5194/gmd-16-5093-2023>
- Geiger, T., Frieler, K., & Bresch, D. N. (2018). A global historical data set of tropical cyclone exposure (TCE-DAT).
- Ghosh, S., Sharma, A., Arora, S., & Desouza, G. (2016). A geoengineering approach toward tackling tropical cyclones over the bay of bengal. *Atmospheric Science Letters*, 17(3), 208–215. <https://doi.org/10.1002/asl.644>
- Hazra, A., Mukhopadhyay, P., Taraphdar, S., Chen, J.-P., & Cotton, W. R. (2013). Impact of aerosols on tropical cyclones: An investigation using convection-permitting model simulation [_eprint: <https://onlinelibrary.wiley.com/doi/pdf/10.1002/jgrd.50546>]. *Journal of Geophysical Research: Atmospheres*, 118(13), 7157–7168. <https://doi.org/10.1002/jgrd.50546>
- Herbener, S. R., Van Den Heever, S. C., Carrió, G. G., Saleeby, S. M., & Cotton, W. R. (2014). Aerosol indirect effects on idealized tropical cyclone dynamics. *Journal of the Atmospheric Sciences*, 71(6), 2040–2055. <https://doi.org/10.1175/JAS-D-13-0202.1>

- Hersbach, H., Bell, B., Berrisford, P., Hirahara, S., Horányi, A., Muñoz-Sabater, J., Nicolas, J., Peubey, C., Radu, R., Schepers, D., Simmons, A., Soci, C., Abdalla, S., Abellan, X., Balsamo, G., Bechtold, P., Biavati, G., Bidlot, J., Bonavita, M., . . . Thépaut, J.-N. (2020). The ERA5 global reanalysis. *Quarterly Journal of the Royal Meteorological Society*, 146(730), 1999–2049. <https://doi.org/10.1002/qj.3803>
- Holland, G. J. (1980). An analytic model of the wind and pressure profiles in hurricanes. *Monthly Weather Review*, 108, 1212–1218.
- Intergovernmental Panel On Climate Change (IPCC). (2022, May 19). *The ocean and cryosphere in a changing climate: Special report of the intergovernmental panel on climate change* (1st ed.). Cambridge University Press. <https://doi.org/10.1017/9781009157964>
- Jiang, B., Huang, B., Lin, W., & Xu, S. (2016). Investigation of the effects of anthropogenic pollution on typhoon precipitation and microphysical processes using WRF-chem. *Journal of the Atmospheric Sciences*, 73(4), 1593–1610. <https://doi.org/10.1175/JAS-D-15-0202.1>
- Khain, A., Cohen, N., Lynn, B., & Pokrovsky, A. (2008). Possible aerosol effects on lightning activity and structure of hurricanes. *Journal of the Atmospheric Sciences*, 65(12), 3652–3677. <https://doi.org/10.1175/2008JAS2678.1>
- Kossin, J. P., & Sitkowski, M. (2012). Predicting hurricane intensity and structure changes associated with eyewall replacement cycles. *Weather and Forecasting*, 27(2), 484–488. <https://doi.org/10.1175/WAF-D-11-00106.1>
- Lee, J., Seifert, P., Hashino, T., Maahn, M., Senf, F., & Knoth, O. (2024). Simulations of the impact of cloud condensation nuclei and ice-nucleating particles perturbations on the microphysics and radar reflectivity factor of stratiform mixed-phase clouds [Publisher: Copernicus GmbH]. *Atmospheric Chemistry and Physics*, 24(10), 5737–5756. <https://doi.org/10.5194/acp-24-5737-2024>
- Liang, Z., Ding, J., Fei, J., Cheng, X., & Huang, X. (2021). Direct/indirect effects of aerosols and their separate contributions to typhoon lupit (2009): Eyewall versus peripheral rainbands. *Science China Earth Sciences*, 64(12), 2113–2128. <https://doi.org/10.1007/s11430-020-9816-7>
- Lin, W., Xu, S., & Sui, C.-H. (2011). A numerical simulation of the effect of the number concentration of cloud droplets on typhoon chanchu. *Meteorology and Atmospheric Physics*, 113(3), 99–108. <https://doi.org/10.1007/s00703-011-0152-x>
- Lohmann, U., & Feichter, J. (2005). Global indirect aerosol effects: A review. *Atmos. Chem. Phys.*

- Lohmann, U., Stier, P., Hoose, C., Ferrachat, S., Kloster, S., Roeckner, E., & Zhang, J. (2007). Cloud microphysics and aerosol indirect effects in the global climate model ECHAM5-HAM. *Atmos. Chem. Phys.*
- Lorenz, E. N. (1963). Deterministic nonperiodic flow. *Journal of the Atmospheric Sciences*, *20*, 130–141.
- Montgomery, M., & Smith, R. (2014). Paradigms for tropical cyclone intensification. *Australian Meteorological and Oceanographic Journal*, *64*(1), 37–66. <https://doi.org/10.22499/2.6401.005>
- Neumann, B., Vafeidis, A. T., Zimmermann, J., & Nicholls, R. J. (2015). Future coastal population growth and exposure to sea-level rise and coastal flooding - a global assessment (L. Kumar, Ed.). *PLOS ONE*, *10*(3), e0118571. <https://doi.org/10.1371/journal.pone.0118571>
- NOAA. (2025). *Hurricane preparedness - hazards* [National hurricane center] [institution: NOAA]. Retrieved July 31, 2025, from <https://www.nhc.noaa.gov/prepare/hazards.php>
- Rosenfeld, D., Khain, A., Lynn, B., & Woodley, W. L. (2007). Simulation of hurricane response to suppression of warm rain by sub-micron aerosols. *Atmos. Chem. Phys.*
- Rosenfeld, D., Woodley, W. L., Khain, A., Cotton, W. R., Carrió, G., Ginis, I., & Golden, J. H. (2012). Aerosol effects on microstructure and intensity of tropical cyclones [Publisher: American Meteorological Society]. *Bulletin of the American Meteorological Society*, *93*(7), 987–1001. <https://doi.org/10.1175/bams-d-11-00147.1>
- Segal, Y., & Khain, A. (2006). Dependence of droplet concentration on aerosol conditions in different cloud types: Application to droplet concentration parameterization of aerosol conditions. *Journal of Geophysical Research: Atmospheres*, *111*, 2005JD006561. <https://doi.org/10.1029/2005JD006561>
- Seifert, A., & Beheng, K. D. (2006). A two-moment cloud microphysics parameterization for mixed-phase clouds. part 1: Model description. *Meteorology and Atmospheric Physics*, *92*(1), 45–66. <https://doi.org/10.1007/s00703-005-0112-4>
- Skamarock, W. C., Klemp, J. B., Dudhia, J., Gill, D. O., Liu, Z., Berner, J., Wang, W., Powers, J. G., Duda, M. G., Barker, D. M., & Huang, X.-Y. (2019). A description of the advanced research WRF model version 4.
- Smith, R. K. (1981). The cyclostrophic adjustment of vortices with application to tropical cyclone modification. *Journal of the Atmospheric Sciences*, *38*, 2021–2030.
- Smith, R. K., & Montgomery, M. T. (2008). The fundamental role of buoyancy in tropical-cyclone intensification.

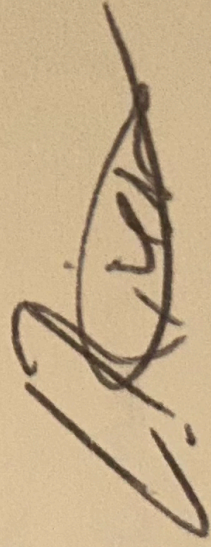
- Smith, R. K., & Montgomery, M. T. (2010). Hurricane boundary-layer theory: Hurricane boundary-layer theory. *Quarterly Journal of the Royal Meteorological Society*, 136(652), 1665–1670. <https://doi.org/10.1002/qj.679>
- SwissRe. (2023, December 14). *Tropical cyclones: Natural catastrophes in focus / swiss re*. Retrieved July 31, 2025, from <https://www.swissre.com/risk-knowledge/mitigating-climate-risk/tropical-cyclones.html>
- Willoughby, H. E., Jorgensen, D. P., Black, R. A., & Rosenthal, S. L. (1985). Project STORM-FURY: A scientific chronicle 1962–1983. *Bulletin of the American Meteorological Society*, 66(5), 505–514. [https://doi.org/10.1175/1520-0477\(1985\)066<0505:PSASC>2.0.CO;2](https://doi.org/10.1175/1520-0477(1985)066<0505:PSASC>2.0.CO;2)
- Willoughby, H., Clos, J., & Shoreibah, M. (1981). Concentric eye walls, secondary wind maxima, and the evolution of the hurricane vortex. *Journal of the Atmospheric Sciences*, 39, 395–411.
- Zängl, G., Reinert, D., Rípodas, P., & Baldauf, M. (2015). The ICON (ICOsahedral non-hydrostatic) modelling framework of DWD and MPI-m: Description of the non-hydrostatic dynamical core [_eprint: <https://onlinelibrary.wiley.com/doi/pdf/10.1002/qj.2378>]. *Quarterly Journal of the Royal Meteorological Society*, 141(687), 563–579. <https://doi.org/10.1002/qj.2378>
- Zhang, H., McFarquhar, G. M., Saleeby, S. M., & Cotton, W. R. (2007). Impacts of saharan dust as CCN on the evolution of an idealized tropical cyclone. *Geophysical Research Letters*, 34(14), 2007GL029876. <https://doi.org/10.1029/2007GL029876>
- Zhao, C., Lin, Y., Wu, F., Wang, Y., Li, Z., Rosenfeld, D., & Wang, Y. (2018). Enlarging rainfall area of tropical cyclones by atmospheric aerosols. *Geophysical Research Letters*, 45(16), 8604–8611. <https://doi.org/10.1029/2018GL079427>
- Zhou, X., & Wang, B. (2011). Mechanism of concentric eyewall replacement cycles and associated intensity change*. *Journal of the Atmospheric Sciences*, 68(5), 972–988. <https://doi.org/10.1175/2011JAS3575.1>

5 Acronyms

- CCN: Cloud Condensation Nuclei
- CDNC: cloud droplet number concentration
- ICON: Icosahedral Nonhydrostatic Model
- q_c : Specific cloud water
- q_i : Specific ice content
- RMW: Radius of maximum wind
- SLP: sea level pressure
- SST: sea surface temperatures
- TC: tropical cyclone
- UTC: Coordinated Universal Time
- v_{\max} : maximum sustained winds
- θ_e : Equivalent potential temperature

Personal Declaration

I hereby declare that the submitted thesis is the result of my own, independent work. All external sources are explicitly acknowledged in the thesis.

A handwritten signature in dark ink, appearing to be 'L. R. K.', written in a cursive style.

31 July 2025